

Stellar activity with LAMOST - II. Chromospheric activity in open clusters

Xiang-Song Fang,^{*} Gang Zhao, Jing-Kun Zhao and Yerra Bharat Kumar

Key Laboratory of Optical Astronomy, National Astronomical Observatories, Chinese Academy of Sciences, Beijing 100012, China

Accepted 2018 January 22. Received 2018 January 18; in original form 2017 August 9

ABSTRACT

We use the LAMOST spectra of member stars in Pleiades, M34, Praesepe, and Hyades to study how chromospheric activity vary as a function of mass and rotation at different age. We measured excess equivalent widths of $H\alpha$, $H\beta$, and $Ca\ II\ K$ based on estimated chromospheric contributions from old and inactive field dwarfs, and excess luminosities are obtained by normalizing bolometric luminosity, for more than 700 late-type stars in these open clusters. Results indicate two activity sequences in cool spot coverage and $H\alpha$ excess emission among GK dwarfs in Pleiades and M dwarfs in Praesepe and Hyades, paralleling with well known rotation sequences. A weak dependence of chromospheric emission on rotation exists among ultra fast rotators in saturated regime with Rossby number $Ro \lesssim 0.1$. In the unsaturated regime, chromospheric and coronal emission show similar dependence on Ro , but with a shift toward larger Ro , indicating chromospheric emission gets easily saturated than coronal emission, and/or convective turnover time-scales based on X-ray data do not work well with chromospheric emission. More interestingly, our analysis show fully convective slow rotators obey the rotation-chromospheric activity relation similar to hotter stars, confirming the previous finding. We found correlations among $H\alpha$, $H\beta$, and $Ca\ II\ K$ emissions, in which $H\alpha$ losses are more important than $Ca\ II\ K$ for cooler and more active stars. In addition, a weak correlation is seen between chromospheric emission and photospheric activity that shows dependency on stellar spectral type and activity level, which provides some clues on how spot configuration vary as a function of mass and activity level.

Key words: stars: activity – stars: chromospheres – stars: late-type – stars: rotation

1 INTRODUCTION

Stellar magnetic activity, triggered by magnetic fields and maintained by a magnetic dynamo, is an ubiquitous phenomenon in late-type stars. Such activity includes a variety of phenomena, e.g., appearance of cool star-spots that are thought to be the fingerprints of emergent magnetic lines on the photosphere; the chromospheric and coronal heating that are responsible for excess chromospheric emissions and thermal X-rays, respectively; impulsive events like flares; and other solar phenomena.

Stellar mass and rotation are thought to be two main basic parameters that affect the dynamo configuration and thus the properties of stellar magnetic activity. On the other hand, the loss of stellar angular momentum through the magnetized stellar wind depends on the magnetic field configuration on stellar surface (Gallet & Bouvier 2013). As

the star brakes due to angular momentum loss, its magnetic field weakens (or the efficiency of the dynamo decreases), and thus activity decays. The correlations between rotation, activity and age are evident from observations of various tracers of activity, e.g., the rotation-activity connection is found based on stellar X-ray emissions (e.g. Pizzolato et al. 2003; Mamajek & Hillenbrand 2008; Wright et al. 2011; Reiners, Schüssler & Passegger 2014), chromospheric $Ca\ II\ HK$ emissions (e.g. Noyes et al. 1984; Mamajek & Hillenbrand 2008) and $H\alpha$ emissions (e.g. Stauffer et al. 1997; Douglas et al. 2014; Newton et al. 2017), and photospheric activity indicator such as cool spot fractional coverage (Fang et al. 2016, hereafter Paper I). The connection between rotation and activity among cool stars directly allows us to understand the nature of the magnetic dynamo in these stars, however, such connection appears to be sensitive to tracers of activity, e.g., chromospheric emission show different dependency on rotation compared to coronal X-ray emission (Douglas et al. 2014).

* E-mail: xsfang@bao.ac.cn

Chromospheric activity (hereafter CA) compasses a wide range of phenomena that produce excess emission (e.g., Ca II and Balmer lines) with respect to a radiative equilibrium atmosphere, stemming largely from changes in their magnetic field (see a comprehensive review on this topic by Hall 2008). Thanks to classic work of Mount Wilson Observatory Ca II HK long-term observations that are operated from 1966 through 2003, for the initial purpose of searching stellar analogues of the solar cycle (Wilson 1968), wherein variety of CA properties including chromospheric variations are explored (Wilson 1978; Baliunas et al. 1995, 1998), e.g., the well-known CA long-term variation patterns (cyclic variation, irregular variation, flat or little variation). What followed was a series of attempts trying to gain the general understanding (statistical characters) of CA among nearby late-type stars, e.g., statistical studies based on chromospheric emissions at the core of Ca II H and K lines among nearby FGK field stars (Henry et al. 1996; Gray 2003, 2006), confirmed the bi-modal distribution in stellar activity (Vaughan & Preston 1980); West et al. (2004, 2008) investigate the fraction of active stars as a function of spectral type and the vertical distance from the Galactic plane, based on a large sample of nearby M-type stars using H α emission line as an activity indicator.

Compared to field stars, open cluster members have an advantage for studying CA properties in light of rotation-activity-age connection due to their homogeneity in age and chemical composition. Therefore, CA in several open clusters got special attention, e.g., the young open cluster Pleiades (Soderblom et al. 1993) and NGC 2516 (Jackson & Jeffries 2010), the median-age open cluster Hyades (Stauffer et al. 1991, 1997) and Praesepe (Douglas et al. 2014). Based on these investigations a general picture is drawn that CA also varies as a function of both stellar mass and rotation. However, due to the limitation of sample stars used in previous studies in terms of mass coverage and available rotation periods (e.g., Pleiades), the behaviours of CA with respect to stellar mass changes and rotation is still not well understood, which demands further investigation on this issue.

LAMOST (Cui et al. 2012) observed millions of stellar spectra for cool stars in our Milky Way (Liu et al. 2015), and more and more stars' rotation periods become available thanks to recent and on-going photometric surveys, e.g., for ~ 1000 Pleiades members (Hartman et al. 2010; Rebull et al. 2016), both of which allow us to initiate systematic study of CA among low mass stars in different population. In Paper I, we found that almost all Pleiades members show excess emission in various indicators (e.g., Ca II HK, H α , H β , Ca I $\lambda 4226$, Mg I b triplet, Na I D lines, and Ca II IRT lines, see Figure 7 and 8 in Paper I) relative to old and inactive field stars, indicating they are chromospherically active. In this paper, we continue to investigate their CA properties in detail among members of nearby open clusters including Pleiades, M34, Praesepe and Hyades by focusing on three chromospheric indicators: H α , H β and Ca II K lines. We examined their incidence and strength of chromospheric activity as a function of effective temperature, and checked the correlation between activity and rotation. We also investigated the relationship amongst these three chromospheric indicators, and the relations between chromospheric emission and several manifestations of magnetic activity in different stellar atmosphere layers (cool spot coverage, light

variation amplitude, and coronal emission), which holds key clues not only to the configuration of the magnetically active region on the stellar surface but also to the magnetically heating processes in stellar outer atmosphere.

2 DATA AND SAMPLE

2.1 LAMOST DR3

The LAMOST, characterized by both wide field of view (5 deg in diameter) and large effective aperture of ~ 4 m, is a reflecting Schmidt telescope located at the Xinglong Observatory, China. LAMOST spectra are obtained in low resolution $R \approx 1800$ (e.g., ~ 3.6 Å around 6500 Å) (see Zhao et al. 2006, 2012; Luo et al. 2015, for more details).

The LAMOST Data Release 3 (DR3) was made available to the Chinese astronomical community and international partners during December 2015, containing nearly 5.3 million stellar spectra that were collected from pilot survey through three years regular survey (autumn 2011 to summer 2015). LAMOST stellar parameter pipeline (LASP) provides the stellar parameters like effective temperature (T_{eff}), surface gravity ($\log g$), metallicity ($[\text{Fe}/\text{H}]$) and radial velocity (RV) for ~ 3.2 million stellar spectra of AFGK stars whose spectra meet the signal-to-noise ratio criterion (e.g., g -band SNR of $\text{SNR}_g \geq 15$ and $\text{SNR}_r \geq 6$ for the bright and dark nights, respectively) (Wu et al. 2011; Luo et al. 2015). In addition, DR3 also include a catalogue of ~ 0.3 million M-type stars.

2.2 Sample stars

We have selected four nearby open clusters with a range of ages from 100 to 700 Myr (Pleiades, M34, Praesepe and Hyades), and retrieved the available spectra of good quality from LAMOST DR3 archive.

The Pleiades (Seven Sisters) is a young open cluster with an age of ~ 125 Myr (Stauffer, Schultz & Kirkpatrick 1998) and metallicity of $[\text{Fe}/\text{H}] \sim 0.03$ (Soderblom et al. 2009), at a distance of around 130 pc (e.g., ~ 136 pc; Melis et al. 2014). In addition to LAMOST DR2 archive used in Paper I, DR3 provide spectra for more than 70 targets from the Pleiades potential member catalogues provided by Stauffer et al. (2007) and Bouy et al. (2015) (whose probability more than 75 percent). In total, we selected 378 probable Pleiades members with 458 LAMOST spectra having signal-to-noise ratio in r -band $\text{SNR}_r > 10$.

M34 (NGC 1039) has an age of about 220 Myrs (see Meibom et al. 2011, and references therein), locates at a distance of ~ 470 pc toward the galactic anti-centre (Jones & Prosser 1996). M34 has metallicity close to solar, $[\text{Fe}/\text{H}] \sim 0.07$ (Schuler et al. 2003). Jones & Prosser (1996) provided proper motion membership probability analysis for more than 600 stars with brightness down to $V \sim 16.2$ in the M34 field, wherein, the cooler members tend to have lower membership probability due to the faintness, e.g., the typical probability of faint stars with $V > 15$ ($\sim K2$ and cooler) is ~ 40 percent, while the brighter members have probabilities close to 100 percent. We selected candidate M34 members with membership probability greater than 40 percent. However, real cool members might be excluded in this criterion.

Table 1. Basic information about the sample stars in current work

Cluster	d (pc)	Age (Myr)	[Fe/H]	E(B-V) (mag)	Sample ^a
Pleiades	136	~125	+0.03	0.03 ^b	378(458), 231
M34	470	~220	+0.07	0.07	45(49), 21
Praesepe	184	~650	+0.16	0.027	176(227), 76
Hyades	46	~650	+0.11	0.001	142(197), 24

^a total number of stars (spectra), and those with rotation period.

^b there is significant differential extinction in the Pleiades, see Soderblom et al. (1993).

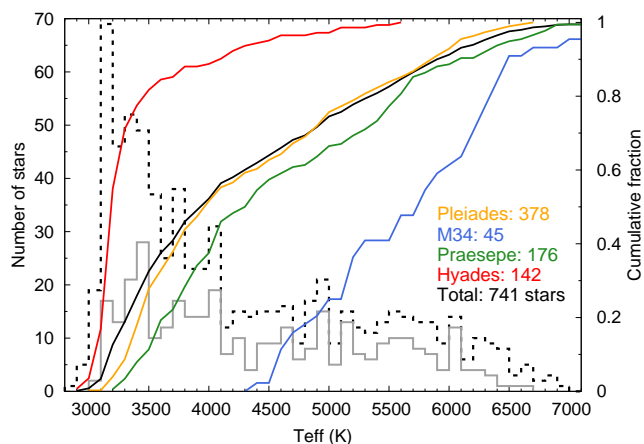


Figure 1. Distribution of the sample stars as a function of temperature. The dashed black line shows the distribution for total sample stars, while the grey line represents these stars for which rotation period is now known. The solid lines with different colours correspond to cumulative fraction profiles (right y-axis).

To collect more member stars, in particular at cooler end, we chose periodic variables detected in M34 (Irwin et al. 2006; James et al. 2010; Meibom et al. 2011), considering them as younger and more active. Unfortunately, only a small number of cool stars in the vicinity of M34 field have been observed by LAMOST (DR3), partly due to their faintness. In total, we collected 45 candidates that have LAMOST spectra with $\text{SNR}r > 10$, most of which are FG-type stars.

The Hyades is the nearest open cluster at a distance of about 46 pc (Perryman et al. 1998), and has solar metallicity $[\text{Fe}/\text{H}] \sim 0.1$ (Taylor & Joner 2005; Carrera & Pancino 2011). The Praesepe (NGC 2632; the Beehive Cluster) has a distance of 180-190 pc (e.g. An et al. 2007; van Leeuwen 2009) and a metallicity of $[\text{Fe}/\text{H}] \sim 0.16$ (Carrera & Pancino 2011; Yang et al. 2016). The Hyades and Praesepe are both part of the Hyades supercluster, and seem to share an intermediate-age around 600-800 Myr (Perryman et al. 1998; Fossati et al. 2008; Brandt & Huang 2015). We adopt the membership catalogue provided by Douglas et al. (2014) for this two clusters, and retrieved 197 spectra for 142 Hyades candidates, and 227 spectra for 176 candidates of Praesepe from LAMOST DR3 archive with $\text{SNR}r > 10$.

Fig. 1 and Table 1 show the summary of total sample (741 stars), and easy to note that more than half (~ 60 per cent) of them are late K- and M-type stars.

3 QUANTIFYING CHROMOSPHERIC ACTIVITY

It is well known that enhanced emission of $\text{H}\alpha$, produced by collisional excitation in the relatively dense chromospheres of low-mass dwarf stars, is the strongest and widely-used activity indicator (e.g. Stauffer & Hartmann 1986; Soderblom et al. 1993; West et al. 2004, 2015; Newton et al. 2017). In this work, $\text{H}\alpha$ line was used as main chromospheric activity indicator, considering that more than 50 percent of our sample stars are late K- and M-type stars (see Fig. 1). However, we also investigated the behaviours of other two activity indicators, Ca II K and $\text{H}\beta$ lines.

3.1 Excess equivalent width

The equivalent widths were measured from RV-corrected spectra of all sample stars. For FGK dwarfs, we adopted RV values derived by LASP, while we measured RVs for M dwarfs following methodology described in Paper I. The equivalent widths of $\text{H}\alpha$ line (hereafter $\text{EW}_{\text{H}\alpha}$) were measured using the formula (equation 4) in Paper I, where the line was centred at 6563 Å over 12 Å bandpasses and continuum flux was taken to be the average flux between 6547-6557 Å and 6570-6580 Å. The measurements of $\text{EW}_{\text{H}\alpha}$ for entire sample are plotted against effective (quiescent) temperatures (see Appendix D for details) in Fig. 2, wherein the mean values of $\text{EW}_{\text{H}\alpha}$ for inactive reference stars (a large sample of very less active field FGKM dwarfs with solar metallicities over the temperature range 3000 – 6500 K, see Paper I for more details) are treated as the minimum or basal value of chromospheric emissions, and shown as black solid line. It is clear from the figure that the members of Pleiades show higher $\text{EW}_{\text{H}\alpha}$ compared to inactive counterparts. In fact, the correlation between $\text{EW}_{\text{H}\alpha}$ and chromospheric activity level is complex, due to presence of non-monotonic behaviour (Cram & Mullan 1979), e.g., firstly the $\text{H}\alpha$ absorption increases with increase in activity, then fill-in, and eventually appear as emission line. Therefore, among the less active stars at the same temperature, the stronger $\text{H}\alpha$ absorption line indicates its higher activity. In this work, we adapted simple approach by ignoring such non-monotonic effect, and consider excess $\text{EW}_{\text{H}\alpha}$ above the basal value as the tracer of pure chromospheric emission. To determine the excess $\text{H}\alpha$ emission, we calculated the excess equivalent widths (the $\Delta\text{EW}_{\text{H}\alpha}$ in Paper I, hereafter denote as $\text{EW}'_{\text{H}\alpha}$) by subtracting the basal value at the same temperature, $\text{EW}_{\text{H}\alpha, \text{basal}}$, i.e.,

$$\text{EW}'_{\text{H}\alpha} = \text{EW}_{\text{H}\alpha} - \text{EW}_{\text{H}\alpha, \text{basal}}. \quad (1)$$

Similarly, we obtained the excess equivalent widths, $\text{EW}'_{\text{Ca K}}$ and $\text{EW}'_{\text{H}\beta}$, for Ca II K and $\text{H}\beta$ lines, respectively (see Appendix A for details).

3.2 Excess fractional luminosity

As shown in Fig. 2, the strong change of $\text{EW}_{\text{H}\alpha}$ (& $\text{EW}'_{\text{H}\alpha}$) with temperature does not only reflect the intrinsic change of chromospheric activity, but also the effects of the drop in the nearby continuum level. To remove the dependency of the measured $\text{EW}_{\text{H}\alpha}$ on the surrounding continuum level, and to compare the strength of chromospheric activity in

different spectral types, we used the fractional luminosity of H α (normalized with the bolometric luminosity) (e.g. Reid, Hawley & Mateo 1995; West et al. 2004). However, quantifying fractional luminosity for a given line requires a flux-calibrated spectrum and the distance. For all activity indicators in this work, the excess fractional luminosities were derived from the excess equivalent widths using a distance-independent value, χ , the ratio between the continuum flux near the line of interest and the bolometric flux, following commonly used χ -methods (e.g. West et al. 2004). Using the χ ratios of H α line ($\chi_{\text{H}\alpha}$) obtained from the model spectra (see Appendix C), we obtained the H α excess fractional luminosity (denote as $R'_{\text{H}\alpha}$), the ratio of excess H α emission luminosity ($L'_{\text{H}\alpha}$) to the bolometric luminosity (L_{bol}), as follows,

$$R'_{\text{H}\alpha} \equiv \frac{L'_{\text{H}\alpha}}{L_{\text{bol}}} = \chi_{\text{H}\alpha} \times \text{EW}'_{\text{H}\alpha}. \quad (2)$$

In similar way, we estimated Ca II K and H β excess fractional luminosities, $R'_{\text{Ca K}}$ and $R'_{\text{H}\beta}$, respectively (see Appendix A). These values provide the fraction of respective bolometric luminosity emitted from the chromosphere in the lines, and are analogous to the chromospheric Ca II emission ratio R'_{HK} (e.g. Noyes et al. 1984) and R'_{IRT} (e.g. Marsden, Carter & Donati 2009; Jackson & Jeffries 2010).

3.3 Comparison with literature measurements

We compared our EW $_{\text{H}\alpha}$ measurements with Douglas et al. (2014), wherein they measured EW $_{\text{H}\alpha}$ from medium resolution (about two times higher than LAMOST) spectra, for common stars in Hyades and Praesepe (see Fig. 3), and found to be in good agreement. Furthermore, Soderblom et al. (1993) and Soderblom, Jones & Fischer (2001) obtained excess H α emission from high-resolution echelle spectra for about 100 FGK dwarfs in the Pleiades and about 50 FGK dwarfs in the M34, respectively, using a synthetic subtraction technique, i.e., the H α profile of each target star is subtracted by the rotationally broadened H α of inactive counterpart. In Fig. 4 we compared their measurements of excess H α emission with our measurements for common stars in the Pleiades and M34, and found they are in close agreement. However, it seems there still exist systematic offset in fractional luminosity for less active hotter stars with $\log R'_{\text{H}\alpha} \lesssim -4.5$, e.g., our measured $R'_{\text{H}\alpha}$ are ~ 0.2 dex larger. In fact, as discussed in Appendix B, a small error in excess equivalent width would result in larger error in fractional luminosity (e.g., see Table B1), particularly when the excess emission is very weak. In a careful check on the excess equivalent width, we indeed found there is a small offset ($\sim 0.1 \text{ \AA}$, see the upper panel of Fig. 4) that is comparable with the uncertainties due to 100 K uncertainty in temperature (see Table B1).

3.4 Variability in chromospheric emission

The larger scatter in Fig. 3 and Fig. 4 are ofcourse partly from the uncertainties of our measurements. However, we believe that they are mainly related to intrinsic variation in activity, which is well-known for Pleiades members (e.g. Soderblom et al. 1993). To further check the variation in H α

emission, we have plotted EW $_{\text{H}\alpha}$ against the temperature in Fig. 5, in which we show minimum and maximum values of EW $_{\text{H}\alpha}$ for stars having multi-epoch spectra. From the figure it is clear that very cool members show high variation in H α emission, which is evidently larger than H α equivalent width measurement errors, indicating intrinsic variability of chromospheric activity. Also, it shows that more active stars have large equivalent width variations, indicating stars with high level activity suffer more often large variations, which maybe due to short-time scale evolution of active regions or flare-like events.

4 RESULTS AND DISCUSSION

4.1 Chromospheric activity as a function of mass

As shown in top-left panel of Fig. 2, the EW $_{\text{H}\alpha}$ is generally a strong function of stellar effective temperature, i.e., EW $_{\text{H}\alpha}$ increases with decreasing temperature, from H α absorption at $T_{\text{eff}} \sim 6500 \text{ K}$ (EW $_{\text{H}\alpha} \sim -2 \text{ \AA}$) to H α emission at $T_{\text{eff}} \sim 3000 \text{ K}$ (EW $_{\text{H}\alpha} \sim 10 \text{ \AA}$). Such trend in the Pleiades was also observed by Stauffer & Hartmann (1987). The upper envelop of EW $_{\text{H}\alpha}$ vs. T_{eff} profile indicates the activity levels of most active stars at a given temperature, provides the clues on chromospheric cooling effects for stars with different mass. Also, it shows the dependency of the upper envelop on spectral types among Pleiades members, e.g., the EW $_{\text{H}\alpha}$ increases moderately as temperature decreases for late-F and G-type stars ($T_{\text{eff}} \gtrsim 5000 \text{ K}$), and for K-type stars it goes into a plateau where exists a slight increment of EW $_{\text{H}\alpha}$, and then it increases sharply when $T_{\text{eff}} \lesssim 4000 \text{ K}$. However, at the same time, the spread in EW $_{\text{H}\alpha}$ also increases. Such feature is more overt in the middle-left panel of Fig. 2. The lower EW $_{\text{H}\alpha}$ of Pleiades members follow the mean relations of inactive reference stars, which vary with temperature, i.e., from EW $_{\text{H}\alpha} \sim -2.5 \text{ \AA}$ at $T_{\text{eff}} \sim 6500 \text{ K}$ to EW $_{\text{H}\alpha} \sim 0 \text{ \AA}$ at $T_{\text{eff}} \sim 3800 \text{ K}$.

We noticed that some Pleiades G-type members have larger EW $_{\text{H}\alpha}$ values compared to inactive counterparts, indicating they have shallower H α absorption line profile (i.e., the core of the line is filled in). The excess H α emission for all clusters are shown in middle panels of Fig. 2. It is clear from the figure that most of Pleiades candidates show excess emission compared to inactive counterparts, i.e., EW $'_{\text{H}\alpha} > 0$, indicating they are in chromospheric active phase, which is consistent with its young age. However, a small fraction of Pleiades stars have weaker excess H α emission compared to other stars in the same spectral type, e.g., about 40 very low-mass stars with $T_{\text{eff}} < 4000 \text{ K}$ have EW $'_{\text{H}\alpha} < 0.5 \text{ \AA}$, while other members in this temperature regime have evident larger EWs (e.g. EW $'_{\text{H}\alpha} > 2 \text{ \AA}$), making a gap around $T_{\text{eff}} \sim 3500 \text{ K}$ in the diagram. One general interpretation is that these stars may be field dwarfs rather than Pleiades members. We found that about one third of these stars are photometrically single candidate members according to their location on CMDs. To further check their membership, we plotted their RVs distribution in Fig. 6, and found about half of them have RVs from -8 to 20 km s^{-1} suggesting they are likely Pleiades members within 3σ -RV regime by adopting the mean RV value of $\mu \sim 6 \text{ km s}^{-1}$ and a scatter of $\sigma \sim 5 \text{ km s}^{-1}$ for Pleiades (see Fig. 6). Several stars (e.g., about

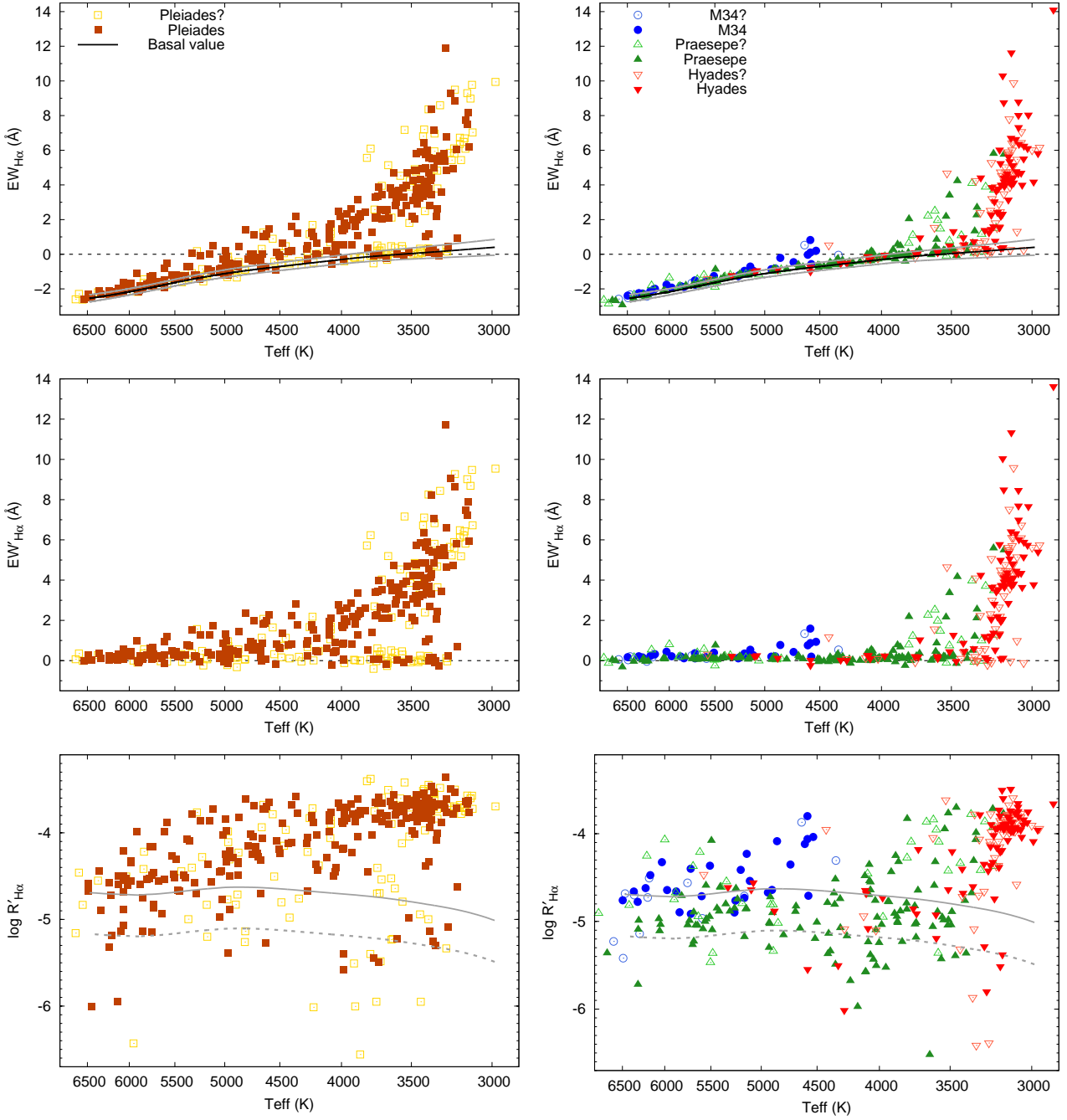


Figure 2. Top: The equivalent widths of H α line for stars in Pleiades (left), and M 34, Praesepe and Hyades (right). Black solid lines show the mean relations for inactive reference stars, upper and lower 3σ to the mean value are shown as grey lines. Filled symbols represent probable single members and open symbols denote probable binary members or non-members. For stars having LAMOST multi-epoch observations, we displayed their average values rather than individual observational values. Middle: The excess equivalent width of H α , $EW'_{H\alpha}$. Bottom: The excess fractional luminosity of H α , $R'_{H\alpha}$, where the grey solid (dashed) lines denote the stars locating in the upper 3σ (σ) regime.

one sixth of them) are probably Pleiades members which pass both the CMD and RV criterion, such as BPL167, DH 668 and DH 908. On the other hand, we noticed that all these less active stars have no rotation periods available till the date. In other words, stars having detected rotation periods show larger activity in the cooler end, which makes the issue complex. Therefore, their memberships and potential

light variation through monitoring indeed need to be further investigated.

The large contrast of continuum flux at H α line between M-type and hotter stars dilutes their larger differences in equivalent widths, which makes the upper envelopes of $R'_{H\alpha}$ among these stars have similar values, e.g., $\log R'_{H\alpha} \sim -3.7$ (see bottom panels of Fig. 2). Still, the upper envelope of

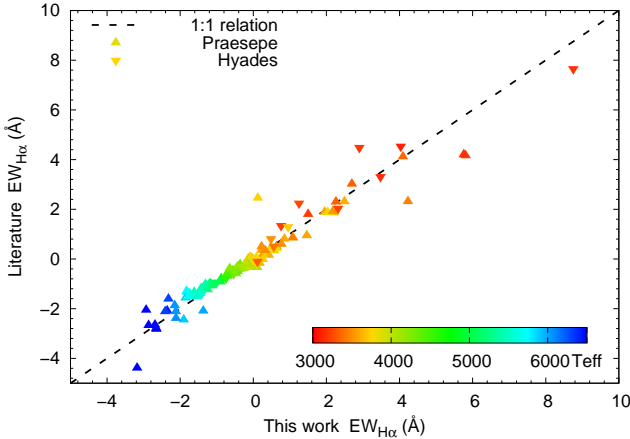


Figure 3. Comparison of our measured $EW_{H\alpha}$ with those of Douglas et al. (2014) for common stars in Hyades and Praesepe.

$R'_{H\alpha}$ in Pleiades M-type stars (e.g., $T_{\text{eff}} \lesssim 3900$ K) show a slight increment with decreasing effective temperature, confirms the previous finding that the low-mass stars in young clusters with age less than 150 Myr show an increase in activity strength ($L_{H\alpha}/L_{\text{bol}}$) toward lower mass (Hawley et al. 1999). Also, previous studies show that later spectral type stars have lower activity level among late M-type stars (e.g. West et al. 2004). Though such trends are evident from $R'_{H\alpha}$ when $T_{\text{eff}} \lesssim 3300$ K, and $R'_{H\beta}$ (see Fig. A1), we can not make a solid conclusion about this issue based on current data.

Another remarkable feature in Fig. 2 is a large scatter of $R'_{H\alpha}$ among hotter Pleiades members. In particular, there evidently are two sequences among GK-type Pleiades candidates, i.e., one sequence of stars have similar activity strengths, and other sequence being with lower activity strength showing an increment towards lower temperature. The largest difference of activity level between these two sequences, e.g., 0.5-0.6 dex in $\log R'_{H\alpha}$ (a factor of about four in $R'_{H\alpha}$), occurs at about 5000 K. Such a difference in activity levels is unlikely due to measurement uncertainties, indicating bi-sequence behaviour among these stars. Therefore, apart from the stellar mass, other factors may play a role in producing the observed dispersion pattern. In fact, we have noticed these two sequences correspond to rotational sequences (see Section 4.2.1).

It is known that the chromospheric activity depends not only on stellar mass but also on age, e.g., the $H\alpha$ emission lasts longer in cooler stars (Stauffer et al. 1991; Hawley et al. 1999). Indeed, Fig. 2 shows a clear age effect on chromospheric activity, i.e., compared to Pleiades, Hyades and Praesepe are typically less active, and M34 with intermediate age between Pleiades and Praesepe/Hyades shows activity levels in-between them. Additionally, the onset of $H\alpha$ direct emission occurs at about $T_{\text{eff}} \sim 5000$ -5500, 4500-5000 K, 4000-4500 K for Pleiades, M34 and Hyades/Praesepe members, respectively. Furthermore, two activity sequences appears among cooler members (e.g., late-K and M-type stars) in Praesepe and Hyades, similar to the feature observed for GK-type members in Pleiades. Interestingly, the members of Praesepe and Hyades with T_{eff} less than 3600 K (spectral type later than M1-M2) have activity levels similar to those of Pleiades active members, indicates

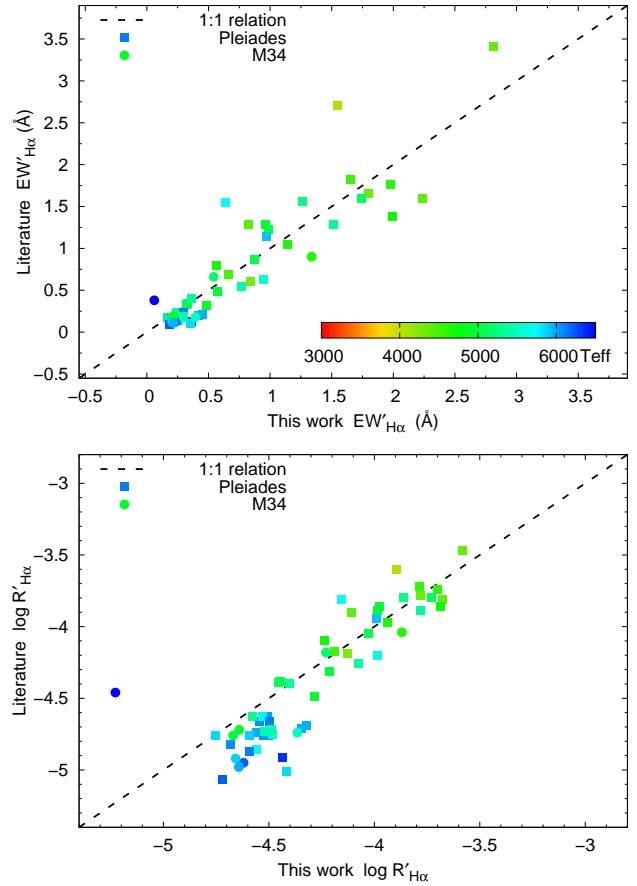


Figure 4. Comparison of $H\alpha$ excess emissions with those of Soderblom et al. (1993) (Pleiades members) and Soderblom, Jones & Fischer (2001) (M34 members) for common stars.

the activity lifetime for M1-M2 type stars is around 600-700 Myr, a value agree with that reported by West et al. (2008). It is possible to get such kind of activity-timescale for earlier spectral type stars by comparing M34 with Pleiades, however, we could not able to provide any solid conclusion due to limited sample of M34 candidates in our data.

4.2 Rotation-activity connection

4.2.1 Rotation and activity sequences

As discussed above, there exist two sequences among GK-type stars in Pleiades, and M-type stars in Praesepe and Hyades in $R'_{H\alpha}$ - T_{eff} diagram, i.e., $H\alpha$ emissions in Pleiades begin to bifurcate at ~ 6000 K and merge again at ~ 4000 K; similar sequences in Praesepe and Hyades appear at ~ 4000 K and disappear at about 3100 K. In order to understand further on this scenario, we provide $R'_{H\alpha}$ as a function of temperature again in Fig. 7, wherein shown only members with known rotation periods. For comparison purpose, we also plot the corresponding rotation period (P_{rot}) distribution in the upper panels, where the P_{rot} values were collected from the literature (see Appendix E). The colour contrast in Fig. 7 denotes the Rossby Number Ro ($Ro = P_{\text{rot}}/\tau$, normalized rotation period by the convective turnover time τ). The τ was estimated from stellar mass (mass were converted from the

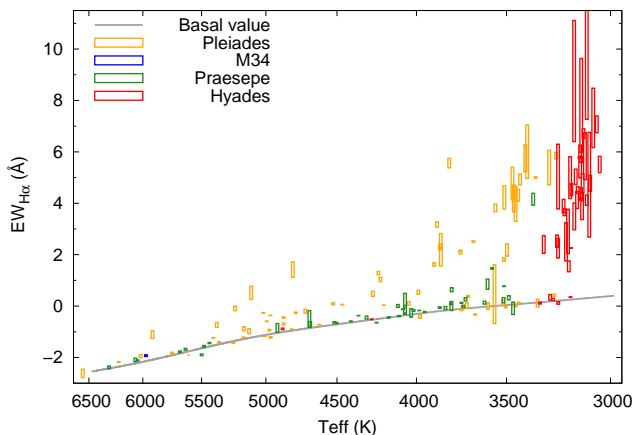


Figure 5. Variation of $EW_{H\alpha}$ for stars having multi-epoch observations. Also shown by grey-colour solid line are the basal values.

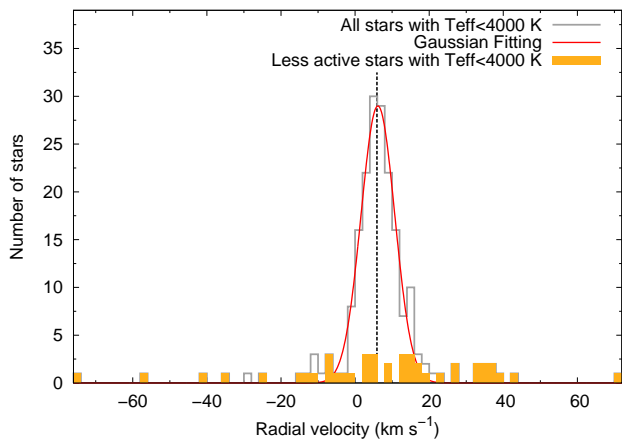


Figure 6. RV distributions of Pleiades candidate members with $T_{\text{eff}} < 4000$ K in inactive regime, shown by the grey line. The red line is a Gaussian fitting, which gives $\mu \approx 6.2 \text{ km s}^{-1}$ and $\sigma \approx 4.6 \text{ km s}^{-1}$. The expected Pleiades RV at 5.9 km s^{-1} provided by Mermilliod, Mayor & Udry (2009) is marked as a black dashed line.

quiescent photosphere temperature using PARSEC models, see Appendix D) using the correlation between convective turnover time and mass, derived by Wright et al. (2011). It is clear that stars in the upper sequence rotate more faster than those in the lower activity sequence.

We noticed that there exist similar features in cool starspot coverages (spot filling factors), as shown in the lower panels of Fig. 7, where the spot filling factors were estimated by modelling their TiO band near 7050 \AA (TiO2) using the standard values obtained based on references stars with solar metallicity (see Paper I for more details). It is clear that there exists a trend for fast rotators among K-type stars in Pleiades having larger spot coverages, and the spot coverages belong to two branches among GK-type Pleiades members. Further, we collected X-ray emission data from literature (Wright et al. 2011; Gondoin 2012) for stars in these open clusters, and found the existence of similar feature with dual sequences, as shown in Fig. 8.

It is known that the open cluster members locate in

three well known regions in the rotation-color diagram (Barnes 2003a), i.e., I (Interface) and C (Convective) sequence stars and gap stars between I and C sequence (e.g., see the top-left panel of Fig. 7). From Fig. 7, we can get a general conclusion that the activity level sequences correspond to the rotation sequences, namely, the more active sequence stars correspond to the C sequence stars, and the stars in less active sequence map to I sequence stars. The dynamo configuration in I sequences may be different with that in C sequences, e.g., a interface dynamo dominates in I sequence stars, and a turbulent or convective dynamo works in C sequence stars, correspondingly causing a large-scale interface magnetic field and a small-scale turbulent field (Barnes 2003a,b). Therefore, such a bifurcation of chromospheric activity of Pleiades GK-type members is probably due to a change in the dynamo configuration. For older open clusters such as Hyades with an age of 600-700 Myr their GK-type member stars rotate slowly and should be in I sequence in the period-colour diagram, but the M members display clearly both I and C sequence (see the top-right panel of Fig. 7). As mentioned above, indeed there is a presence of two $H\alpha$ emission sequences for early and Mid-M stars in Praesepe and Hyades. Moreover, it is clear that the two activity sequences correspond to I- and C-rotation sequences, as shown in Fig. 7. For M34, an open cluster with an age of about 220 Myrs, the two activity sequences should be observed among K-type stars. However, we could not notice such feature due to lack of observational data of the M34 K-type stars.

4.2.2 Rotation-activity correlation

We have investigated the rotation-activity connection in terms of Rossby number Ro , however, it is difficult to judge whether Rossby number is superior to rotation period when modernizing this rotation-activity relation (e.g., see a comprehensive study on this topic by Reiners, Schüssler & Passegger 2014). In Fig. 9 the $R_{H\alpha}$ against Ro is displayed for our sample stars whose periods are available. As expected, it shows two different regimes, saturated and unsaturated, with different dependency of activity on rotation around a turnoff point (e.g., $Ro \sim 0.1$), usually shown by X-ray emissions (e.g. Wright et al. 2011), chromospheric Ca II and $H\alpha$ emissions (e.g. Noyes et al. 1984; Jackson & Jeffries 2010; Douglas et al. 2014; Newton et al. 2017), and cool spot coverages (Fang et al. 2016).

The rotation-activity relationship is often parameterized by a flat region connected to a power law decay, i.e., the activity has constant (saturated) value below a turnoff of Ro (namely Ro_{sat}), and above Ro_{sat} it declines as a power law of Ro , indicates activity is proportional to Ro^β . Wright et al. (2011) found that the decline in coronal emission follow a power-law with $\beta = -2.18$ for $Ro > 0.13$ based on large sample of 824 late-type stars. Furthermore, they derived $\beta = -2.7$ for a set of solar-type stars. However, the chromospheric emissions show a much shallower power law decay for slow rotators, e.g., the first two Ca II IRT excess emissions in early M-type dwarfs in NGC 2516 decreases as a power-law of $\beta \sim -1$ for $Ro \gtrsim 0.1$ (Jackson & Jeffries 2010). Recently, Douglas et al. (2014) derived much shallower power-law with $\beta = -0.73$ for $Ro > 0.11$ in $H\alpha$ emis-

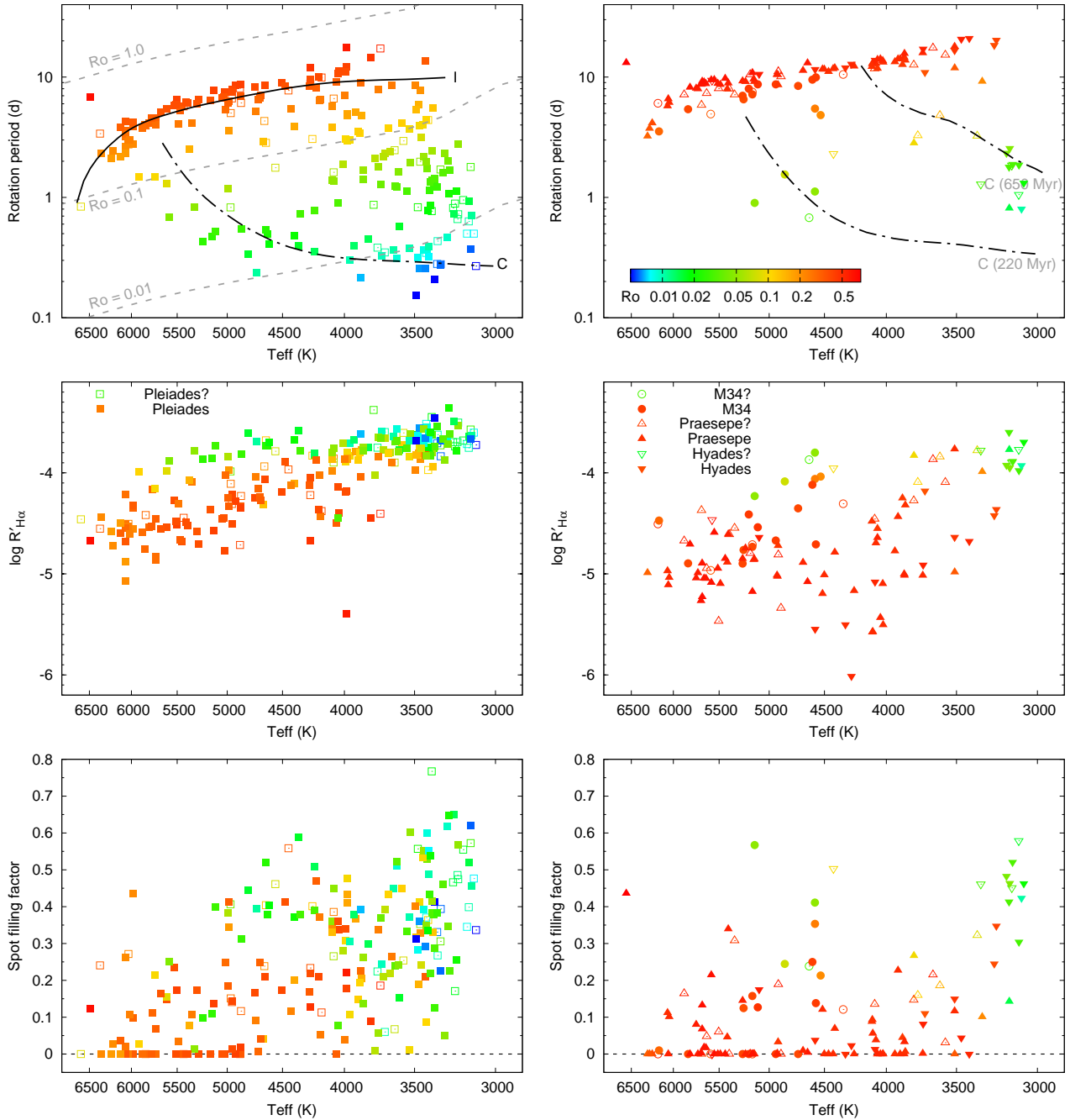


Figure 7. Rotation period (top), $R'_{H\alpha}$ (middle), and spot filling factor (bottom) as a function of T_{eff} for stars with rotation period available. Left: Pleiades. Right: M34, Praesepe and Hyades. The colour gradient indicates Rossby numbers. Over-plotted in top-right panel are contours of constant Rossby numbers ($Ro=0.01, 0.1$ and 1.0 ; grey dashed lines) based on the empirically calibrated mass-convective overturn time relation by [Wright et al. \(2011\)](#). The canonical rotational I/C sequences are illustrated by black lines in top panels.

sions of late K and M dwarfs of Praesepe and Hyades. More recently, [Newton et al. \(2017\)](#) detected a power law index $\beta = -1.7$ with $Ro_{\text{sat}} = 0.21$ in excess H α emission based on large sample of nearby M dwarfs.

The rapid rotators with $Ro \lesssim 0.1$ in Fig. 9 indicates that the chromospheric emissions have similar values shaping a plateau feature (e.g. [Delfosse et al. 1998](#); [Reiners, Joshi & Goldman 2012](#); [Douglas et al. 2014](#); [Newton et al. 2017](#)). Approximately, H α emission saturates

at $\log R'_{H\alpha} \approx -3.7$ dex, while H β and Ca II K emission saturate respectively at $\log R'_{H\beta} \approx -4.1$ dex and $\log R'_{Ca K} \approx -4.0$ dex. The activity level is usually thought to be a constant value in the saturated regime. However, our data shows that the chromospheric emissions still increase slightly as Ro decreases, a phenomenon exists in other activity indicators, e.g., Ca II IR emissions of early M-type members of NGC 2516 ([Jackson & Jeffries 2010](#)). We found

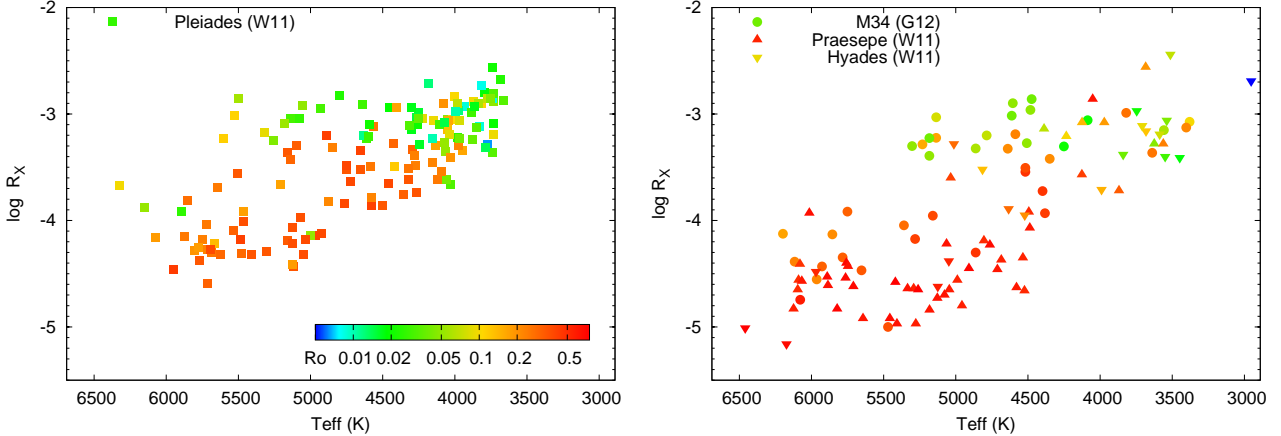


Figure 8. Fractional X-ray emission luminosities R_X as a function of T_{eff} for stars in Pleiades (left), and M34, Praesepe and Hyades (right). These data were collected from literature, as labelled in the panels, where W11: Wright et al. (2011), G12: Gondoïn (2012).

that it can be roughly fitted by some power of Ro , e.g., $R'_{H\alpha} \propto Ro^{-0.2}$ for Pleiades stars with $Ro \lesssim 0.1$, as shown by black dashed line in the top-left panel of Fig. 9, a relationship consistent with that ($L_X/L_{\text{bol}} \propto Ro^{-0.16}$) derived by Reiners, Schüssler & Passegger (2014) based on X-ray emission. A similar increment could be seen in the $H\beta$ emission, e.g., $R'_{H\beta} \propto Ro^{-0.28}$ (the black dashed line in middle-left panel of Fig. 9). We could not see such trend in Ca II K emission in this regime for total sample stars, which maybe due to large uncertainties in $R'_{\text{Ca K}}$ for cooler stars. However, one can see that there also exist a slight increase relation in GK-type stars, e.g., $R'_{\text{Ca K}} \propto Ro^{-0.2}$ (the dashed line in bottom-left panel of Fig. 9). Such a slight slope of the activity-rotation relationship in the saturated regime indicates some unclear dependency of the activity on rotation is remaining even when saturation is reached, as pointed out by Reiners, Schüssler & Passegger (2014).

The activity levels of ultra fast rotating G/K stars are decreasing below the saturation level, a phenomenon known as supersaturation which has been detected in the coronal emission (e.g. Randich et al. 1996; Wright et al. 2011). we found no clear evidence in our sample for any systematic fall in chromospheric activity levels when the Rossby numbers become very small. However, we noticed that the average CA of M-type stars follows a decreasing trend as rotation rate increases at $Ro \lesssim 0.01$ (particularly in terms of the excess Ca II K emission), showing a weak evidence of damped cooling efficiency in ultra fast rotators.

The regime with $Ro \gtrsim 0.1$ are usually thought to be unsaturated regime. At first sight, the activity decreases with increasing Ro , which is expected from qualitative arguments based on the $\alpha\Omega$ -type shell dynamo theory (e.g. Noyes et al. 1984; Charbonneau 2014, and references therein). Moreover, the stars with Ro in the regime of 0.1-0.4 have large scatter in activity with upper envelop near to saturated activity level, which makes it difficult to explain the location of turnoff point. Even worse is the strong dependency of power law with onset of saturation, Ro_{sat} , i.e., β anticorrelates with Ro_{sat} , as seen in Douglas et al. (2014) and Newton et al. (2017). Anyway, we sought to represent the potential trends using the canonical rotation-activity relation (a saturated regime and a power law decay) following

the previous studies, being fitted by eye rather than using any χ^2 -methods. For Pleiades candidate members (see left panels), we found that the saturation may occurs at Ro near to 0.2 rather than the canonical value of 0.1, and a power law is likely in the range of $-2.0 \sim -2.5$, e.g., it can be represented by a relation of $R'_{H\alpha} \propto Ro^{-2.2}$ for $Ro \gtrsim 0.19$, as illustrated by the black solid line in top-left panel of Fig. 9. We found a similar power law decay with Ro_{sat} near to 0.2 in $H\beta$ emissions for the Pleiades sample stars, as illustrated by the black solid line ($R'_{H\beta} \propto Ro^{-2.3}$ for $Ro \gtrsim 0.19$) in middle-left panel of Fig. 9. Compared to these two Balmer emissions, the Ca II K emissions show a slight different trend, i.e., the unsaturated regime start at a larger Ro (e.g., $Ro_{\text{sat}} \gtrsim 0.25$), but appears to be a reasonably fit by a similar power law (an example relation with $\beta = -2.3$ and $Ro_{\text{sat}} = 0.27$ is shown by the black solid line in bottom-left panel).

The results for M34, Hyades and Praesepe are shown in the right panels of Fig. 9. For comparison purpose, in each right panel, we re-plotted the black lines in corresponding left panel. Among these older stars, most hotter stars are slow rotators, in particular members of Praesepe and Hyades, which are in unsaturated regime as expected, and only some M dwarfs in the Praesepe and Hyades and K-type members in M34 are fast rotators (see top panels of Fig. 7) that are occupied in the saturated regime. In the saturated regime, their excess chromospheric emissions increase as Ro decreases similar to Pleiades stars, but systematically having lower level. In the unsaturated regime, they appear to still follow the power law in a similar way as the Pleiades members, but with larger dispersion. However, it seems that Ca II K emission saturates at a larger Ro_{sat} value, e.g., $Ro_{\text{sat}} \gtrsim 0.3$ (alternatively, these stars follow a shallower power laws at the same onset saturation in Pleiades). In top-right panel of Fig. 9, also shown is the relation of $\beta = -0.73$ with $Ro_{\text{sat}} = 0.11$ in dashed grey line, which was derived by Douglas et al. (2014) for M dwarfs with $H\alpha$ in emission in the Praesepe and Hyades. However, our data are inconsistent with their results, our $H\alpha$ data can be fitted by a clearly deeper power law with a larger Ro_{sat} value. The strong degeneracy between β and Ro_{sat} may be a potential contributor. Moreover, Douglas et al. (2014) sample consists of stars with $r' - K \gtrsim 3$ (roughly later than K7) and definite

$H\alpha$ emission, neglected potential less active members with $H\alpha$ in absorption (but in fact having excess emissions such as these GK-type members), which may also accounted for the notable difference between their results and ours. The relation for $\beta = -1.7$ with $Ro_{\text{sat}} = 0.21$ derived by [Newton et al. \(2017\)](#) for nearby M dwarfs also shown in solid grey line in the top-right panel. The Ro_{sat} shown by our $H\alpha$ data is consistent with their value, however, the power law index is slightly deeper than their value.

The transformation between the solar-type stars (with radiative cores and convective envelopes) and fully convective stars takes place roughly in stars of spectral type M3-M4. The interface layer between radiative cores and convective envelopes (known as the tachocline) is believed to play an important role in the generation of the magnetic field in solar-type stars ([Spiegel & Zahn 1992](#)). Therefore, the dynamo mechanism in the fully convective stars such as middle/late M-type stars is expected to be very different because of the absence of a tachocline. However, it is evident that slowly rotating, fully convective stars still show rotation-activity (X-ray emission) connection in the same way similar to solar-type stars ([Wright & Drake 2016](#)). Recently, [Newton et al. \(2017\)](#) found a single relation between excess $H\alpha$ emission and Ro for stars including both early- and late-type M dwarfs, supporting the previous finding. Unfortunately, most M-type stars in our sample are fast rotators (see Fig. 7), and only two slow rotators in Hyades are fully convective candidate stars (marked as large open circles, and see Table 2). To take a simple look at this issue, we picked up LAMOST spectra for 47 slowly rotating M dwarfs ($P_{\text{rot}} > 10$ days, $Mass < 0.6 M_{\odot}$) from the main-sequence *Kepler* targets with known rotation periods provided by [McQuillan, Mazeh & Aigrain \(2014\)](#), and measured their excess CA emissions, as shown by crosses in right panels of Fig. 9 (only 29 of them show excess $H\alpha$ emission). Note that two of them are the fully convective candidates, which were marked with large open circles (but also see Table 2). It is clear that these slowly rotating M dwarfs, including the fully convective candidates, still follow the power law decay that show no evident difference from hotter stars, which is consistent with the finding of [Newton et al. \(2017\)](#), though our results show a slight different power law decay. If this scenario is real, it then suggests that the magnetic dynamo may be similar to that in solar-type stars. [Wright & Drake \(2016\)](#) suggest a common magnetic dynamo in both partially and fully convective stars, supporting those models in which the dynamo originates throughout the stellar convection zone.

4.3 Correlations between activity indicators

The correlations among activity indicators of different temperature layers contain information of overall heating process and systematic deficiencies in these layers ([Güdel 2004](#)). Therefore, the correlations between different chromospheric activity indicators and the relation of excess chromospheric emission with other activity indicators had gained lot of attention (e.g. [Schrijver, Dobson & Radick 1992](#); [Montes et al. 1995, 1996](#); [Martínez-Arnáiz et al. 2011](#)). In fact, this topic need further investigation, e.g., need complex physical models to interpret the correlations, which is beyond the scope of this paper. Our intent here is to merely

investigate the basic observational correlations between different tracers of activity.

4.3.1 $H\alpha$, $H\beta$ and Ca II K

Ca II H&K lines are the most widely used chromospheric activity indicators as their source function are collisionally dominated. $H\alpha$ and $H\beta$ are the two strongest lines among Balmer series, and their excess emissions are formed at the middle chromosphere ([Montes et al. 2004](#)). Our data shows that there exist good correlations of excess emissions of $H\alpha$ to that of $H\beta$ and Ca II K lines, as shown in Fig. 10 and Fig. 11.

Fig. 10 shows a power law correlation (linear relation in log-log scale) between excess equivalent widths of the two Balmer lines, $EW'_{H\alpha}$ and $EW'_{H\beta}$, among the Pleiades stars. We found that it can be represented well by a power law index in the range of 1.2 – 1.4, e.g., $EW'_{H\beta} \propto (EW'_{H\alpha})^{1.3}$, as illustrated by the black dashed line in top-left panel of Fig. 10. For members in M34, Praesepe and Hyades, it also can be represented roughly by the same power law relation, as shown by the black dashed line in top-right panel. It is noticeable that the main trend between $R'_{H\beta}$ and $R'_{H\alpha}$ also roughly linear in log-log scale. Moreover, we found that the power law index is around 1.0, which indicates a linear relation roughly even in linear scale, e.g., $R'_{H\beta} \propto R'_{H\alpha}$, as demonstrated by dashed lines with constant ratios ($R'_{H\alpha}/R'_{H\beta} = 0.5, 1, 2, 4$ and 8, from top to bottom, respectively) in lower panels of Fig. 10. A constant $H\alpha$ to $H\beta$ ratio has been detected in previous studies, e.g., [Reid, Hawley & Mateo \(1995\)](#) found a good linear correlation between the flux emitted at $H\alpha$ and $H\beta$ for low mass stars in the Hyades ($F_{H\alpha} \sim 4.6 \times F_{H\beta}$). However, some late-F or early G-type stars show departures from the general trend, e.g., their $H\beta$ losses seem to be more important than $H\alpha$ losses. In fact, compared to $H\alpha$, $H\beta$ is preferred the higher chromospheric density, e.g., while $H\beta$ enhanced during a flare-like event, the $H\alpha$ is not proportionally increased in strength ([Huenemoerder & Ramsey 1987](#)). Thus the ratio of energy emitted in the $H\alpha$ to $H\beta$ ($E_{H\alpha}/E_{H\beta}$) is widely used as indicator of the presence of flare-like events ([Huenemoerder & Ramsey 1987](#)), and also a diagnostic indicator for discriminating between stellar plagues and prominences ([Hall & Ramsey 1992](#)). The typical value of $E_{H\alpha}/E_{H\beta}$ is around 1 in flare-like events, it then become 4 or larger for RS CVn stars ([Huenemoerder & Ramsey 1987](#)). Therefore, the departure that some earlier type stars with lower $H\alpha$ to $H\beta$ ratios ($R'_{H\alpha}/R'_{H\beta} < 1$) were likely underlying flare/plage-like activities. If this is the real case, then it suggests that these stars preferred to suffer flare events than cooler stars.

It is clear from Fig. 11 that there exist power-law relationship (linear relation in log-log scale) between excess equivalent widths of $H\alpha$ and Ca II K lines. Here we did not attempt any χ^2 fitting but merely sought to reproduce the correlation by eye as before. It can be represented approximately by a power-law index of 1.0 – 1.1, e.g., $EW'_{Ca\ II\ K} \propto (EW'_{H\alpha})^{1.05}$ (see the black dashed lines in upper panels), for which the power-law exponent is slight larger than the value (0.97) derived by [Montes et al. \(1995\)](#) based on a sam-

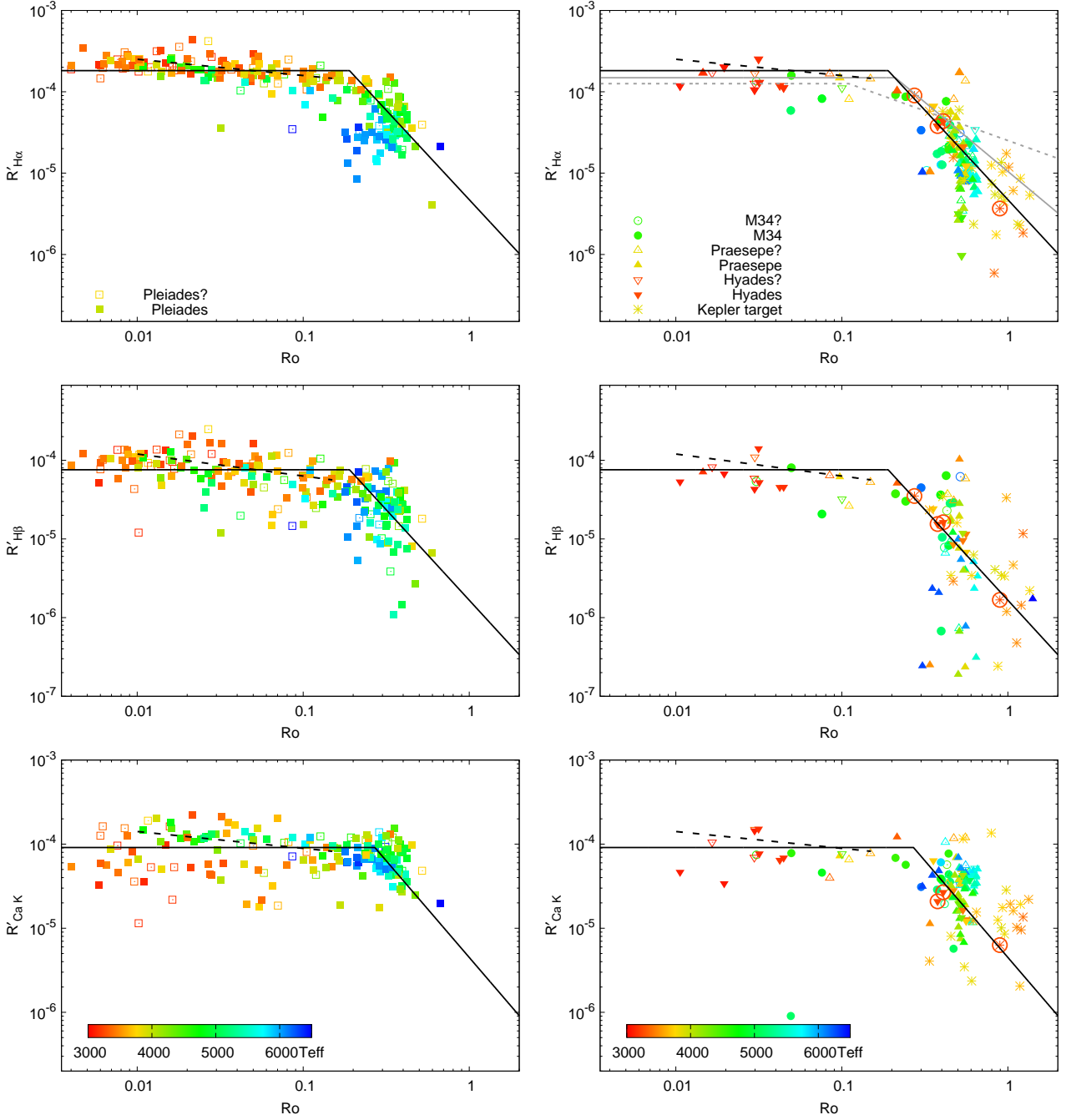


Figure 9. $R'_{H\alpha}$, $R'_{H\beta}$, and $R'_{Ca K}$ vs. Ro for stars in Pleiades (left) and M 34, Praesepe and Hyades (right). The colour gradient represents different effective temperatures. The cross symbols show slowly rotating *Kepler* M dwarfs ($P_{rot} > 10$ days, $Mass < 0.6 M_{\odot}$). The fully convective candidates are marked by large circles. The grey solid and dashed line in top-right panel denote the relation of [Newton et al. \(2017\)](#) and [Douglas et al. \(2014\)](#), respectively.

Table 2. Slow rotating, potential fully convective stars with detected excess emissions in both H α and H β lines

Object name	SpT.	T_{eff} (K)	Mass (M_{\odot})	P_{rot} (days)	Ro	$\log R'_{H\alpha}$	$\log R'_{H\beta}$	$\log R'_{Ca K}$	Note
04202761+1853499	M3.6	3244	0.375	20.3105	0.4079	-4.3609	-4.7871	-4.5722	Hyades
04303385+1444532	M3.5	3257	0.382	18.4100	0.3771	-4.4220	-4.8098	-4.6805	Hyades
KIC 10731839	M3.3	3272	0.362	46.1150	0.8946	-5.4351	-5.7745	-5.2008	<i>Kepler</i> target
KIC 11495571	M3.4	3292	0.374	13.6400	0.2737	-4.0450	-4.4538	–	<i>Kepler</i> target

ple of 51 chromospherically active binaries. The lower panels of Fig. 11 correspond to relations between excess fractional luminosities of Ca II K and H α , which could be represented approximately by a relation of $R'_{\text{Ca K}} \propto (R'_{\text{H}\alpha})^{0.5}$ for GK-type Pleiades stars (see the black dashed lines in lower panels). However, cooler and more chromospherically active stars such as M-type stars do not obey the general relations, showing departure feature of much sharper slope compare to hotter stars. It is illustrated as an example relation $R'_{\text{Ca K}} \propto (R'_{\text{H}\alpha})^{2.0}$ by grey solid lines in the figure, which indicates that H α losses tend to be more important than Ca II K losses for cooler stars that are more active. In fact, previous studies show such departures from the general trend in surface flux-flux relations between H α and other chromospheric indicators among some late-K and M dwarfs, and they are found to be young stars or flare stars being in the X-ray saturation regime (e.g. Martínez-Arnáiz et al. 2011). One can see that the departures hosted in M stars with non-universality trends appear both in young open cluster, Pleiades, and median-age open clusters, Hyades, and most of these stars are indeed in H α emission saturation regime. It has been suggested that the stars deviating from the general relation probably have a different magnetic structure (Martínez-Arnáiz et al. 2011), e.g., nanoflare heating.

4.3.2 H α and photospheric activity

In Fig. 12, we showed the spot filling factor (or fractional spot coverage, f_s) of stars with detected cool spots ($f_s > 0$) in Pleiades as a function of $R'_{\text{H}\alpha}$. The spot coverage of stars have large scatter, which makes harder to say about existence of any believable connections between these two activity indicators. However, the overall trend, in particular among more chromospherically active members (e.g., if we consider stars with $\log R'_{\text{H}\alpha} > -5.0$ and keep aside the outliers at the end of weak H α emission), shows that more active stars tend to have larger spot coverages. We use a Pearson's product-moment correlation analysis to test the statistical significance of the potential connections between f_s and $\log R'_{\text{H}\alpha}$. The Pearson's correlation coefficient $r \approx 0.55$ among stars with $\log R'_{\text{H}\alpha} > -5.0$ indicates that there exist some correlation between spot coverage and chromospheric emission. Compared to hotter stars such as GK-type members, most M-type Pleiades members (see red symbols in Fig. 12) are in H α emission saturation regime, showing a different and slightly tighter trend in the plot, which also evidenced by a stronger positive correlation of $r \approx 0.63$ (for stars with $T_{\text{eff}} < 3900$ K and $\log R'_{\text{H}\alpha} > -4.0$). It is clear that such non-universality feature is very similar to the relation between chromospheric emissions of H α and Ca II K, as discussed above. Note that the uncertainties are larger in determination of spot coverages for M-type star as discussed in Paper I, and the correlation showed in the plot need to be further investigated, which puts a caution for further discussion based on these features.

The amplitude of light variation due to spot rotational modulation carries information of inhomogeneity in the stellar surface, thus acts as another indicator of photospheric activity, e.g, the light variation become larger with increase in chromospheric activity among Sun-like stars (e.g. Lockwood, Skiff & Radick 1997; Radick et al. 1998;

Lockwood et al. 2007) and M dwarfs (e.g. Newton et al. 2017). The amplitudes of periodic light variation versus excess H α emissions for Pleiades candidates with detected rotation period are shown in Fig. 13, where the r -band peak-to-peak photometric amplitudes A_r were derived by Hartman et al. (2010) based on the HATNet light curves. On the whole, there is a trend showing larger chromospheric emission corresponds to larger light variation, however, the dispersion is large as shown in the left panel. The Pearson's correlation coefficient in log-log scale is $r \sim 0.71$ (with a p -value of $< 2.2 \times 10^{-16}$). The right panel of Fig. 13 is analogous to the left panel, wherein the amplitude of variation (between 10 percent and 90 percent of the distribution of points) A_{K2} is derived by Rebull et al. (2016) based on K2 observations. We noticed some additional features from this panel. The correlation is weaker that is evidenced by a smaller value of $r \sim 0.47$ ($p \sim 1.4 \times 10^{-9}$). And there exist systematic offset between the A_{K2} and A_r for very cool stars (see red symbols). By neglecting the very cool stars with $T_{\text{eff}} < 3900$ K, the correlation become tighter ($r \sim 0.62$, $p \sim 1.9 \times 10^{-10}$). Previous studies show that the short-term photometric variability (mainly due to rotational spot modulation) in less active Sun-like stars can be related to their average level of chromospheric activity by a power law (e.g. Radick et al. 1998). The Pleiades GK-type members in the unsaturated regime are roughly linear on the log-log scale plot, indicating a power law relation. On the other hand, M dwarfs still follow the general trend of more active stars showing higher levels of photometric variability (e.g. Newton et al. 2017). As most of the Pleiades M-type stars are in saturated chromospheric activity regime, there is no believable trend among these very cool stars with $T_{\text{eff}} < 3900$ K in both panels (left: $r \sim 0.21$, $p \sim 0.12$; right: $r \sim 0.08$, $p \sim 0.50$), which probably due to their very high activity levels. In fact, the chromospheric activity levels vary in short term (as shown in Fig. 5), and long term such as cyclic variation (e.g. Baliunas et al. 1995), thus the panels of Fig. 13 actually represents a snapshot of stellar variability. Moreover, the pattern and evolution of spots, and stellar inclination (the orientation angle of the axis of rotation relative to our line of sight) could effect the light variation pattern and contaminate the potential relation between chromospheric emission and light variation, thus the feature shown in this figure is only instructive rather than conclusive.

4.3.3 H α and coronal X-ray emission

To investigate the relation between chromospheric heating and coronal emission, we have taken R_X ($= L_X/L_{\text{bol}}$) from Wright et al. (2011) for common Pleiades candidate members, and plotted against $R'_{\text{H}\alpha}$ in Fig. 14. A simple linear fit in log scale indicated that the power law index is around 1.44, e.g., $R_X \propto (R'_{\text{H}\alpha})^{1.44}$ (see black dashed line in Fig. 14). A slight steeper correlation of coronal and chromospheric emission flux with a power of 1.5-1.7 based on magnetic induced excess flux in the Ca II H&K lines was reported (Schrijver, Dobson & Radick 1992; Güdel 2004, and further references cited therein). Such a non-linearity in the chromospheric-coronal flux-flux correlation may be a manifestation of the chromospheric radiative losses (Güdel 2004). The correlation between H α emission and X-ray emission in-

icates that the formation process may be same or at least correlated.

4.4 What can we learn from the results

The different onsets of saturation in various chromospheric activity indicators suggests the existence of transition regime at Ro range of 0.1-0.4, which connects the unsaturated and saturated regime with steep and shallower power law, respectively. In fact, [Gondoin \(2012, 2013\)](#) showed the evidence for transition from saturated to non-saturated X-ray emission that occurs at Ro between ~ 0.13 and 0.4 in open clusters M34 and M35. Indeed, this transition scenario could describe the scatter in Ro region of 0.1-0.4. However, such scenario fails to explain the whole observational features in this Ro regime, e.g. the Ca K emission that shows a clear rotation-activity relationship, suggests the investigation towards other unknown parameters or the activity behaviours in this regime.

In addition, the chromospheric emission follow the similar (slight shallower) power laws in the unsaturated regime compared to coronal X-ray emission, but appears to be shifted to a larger Ro_{sat} value, which indicates that chromospheric emission gets easily saturated at a given rotation rate than coronal emission. Alternatively, it may suggest that the convective overturn time scale, empirically derived based on X-ray emission ([Wright et al. 2011](#)), is not suitable for chromospheric emission.

A corresponding relation between the saturated/non-saturated regimes of X-ray emission and the C/I rotation sequences among late-type stars has been reported in literature (e.g. [Barnes 2003b](#); [Gondoin 2012, 2013](#)). In our work, we detected a similar correspondence in $H\alpha$ emission among cool stars in Pleiades, Praesepe and Hyades, as discussed in previous sections. [Barnes \(2003b\)](#) and [Gondoin \(2012\)](#) suggested such transition from the saturated to the non-saturated regime of activity is the manifestation of a dynamo transition, e.g., from a turbulent dynamo to an interface-type dynamo. [Durney, De Young & Roxburgh \(1993\)](#) showed a candidate turbulent dynamo, which can generate small-scale turbulent magnetic field in late-type stars, and have a weak dependency on rotation. Such a turbulent dynamo can naturally explain the weak dependency of activity on rotation among fast rotators in the saturation regime. Moreover, the generation of small-scale magnetic field supports some observational behaviour shown by very active stars, e.g., large spot coverage of stars in young open clusters may be due to many small and randomly located spots on the stellar photosphere ([Jackson & Jeffries 2012, 2013](#); [Fang et al. 2016](#)), and the possibility of multiple small flares such as nanoflares that might be responsible for the departures of relation between various chromospheric emissions among very active late-K and M dwarfs reported by previous studies and discussed above in current work. We thus conclude that a turbulent-like dynamo dominates in fast rotating cool stars in the saturated regime.

5 CONCLUSION

We have quantified CA (excess emissions in $H\alpha$, $H\beta$, and Ca II K lines) in more than 700 stars from various open

clusters including Pleiades, M34, Praesepe and Hyades, using LAMOST DR3 spectra. The CA was investigated as a function of stellar parameters: mass, age, and rotation. We also analysed the correlation between activity indicators of various atmosphere layers.

CA was found to be overall increased as temperature decreases, showing a mass-dependency, which partially could be due to deeper convective zones in cooler stars. CA also shows a clear age-dependence, i.e., activity level of GK-type stars declines steadily from 100 Myrs to about 700 Myrs. Additionally, we found that the activity lifetime for M1-M2 type stars is around 600-700 Myr, which is consistent with previous studies. More interestingly, there appear two sequences among Pleiades GK-type stars in activity (spot coverage, chromospheric and coronal emission)- T_{eff} diagram, paralleling with well known rotation sequences. We also found the existence of similar sequences in Praesepe and Hyades M-type members.

We found CA is correlated with rotation in the unsaturated regime, following a power law with power of β between -2 and -2.5, which is marginally consistent with results from X-ray emissions, but with a larger turnoff point of Ro (e.g., $Ro_{\text{sat}} \sim 0.2 - 0.3$). A weak dependency of CA on rotation is noticed in the saturated regime of activity ($Ro \lesssim 0.1$), e.g., a slight increase as Ro decreases (a power law with $\beta \approx 0.2$), peaks around $Ro \sim 0.01$, and decrease when Ro decreases for $Ro \lesssim 0.01$. In addition, our analysis confirms the previous finding that slowly rotating, fully convective stars also follow the activity-rotation trend like the hotter stars.

We found a good linear correlation between the luminosity emitted at $H\alpha$ and $H\beta$. The relations from excess emission of $H\alpha$ to that Ca II K lines confirms that cool stars follow two different power law flux-flux relationships. We also found weak correlation between chromospheric emission and photospheric activity indicators (cool spot filling factor and light variation amplitude), however, it shows dependency on spectral type and activity level, which provides clues on how spot configuration vary as a function of mass and activity. A good correlation between chromospheric and coronal emissions was also detected that confirms previous findings.

ACKNOWLEDGEMENTS

We thank the referee for his/her observant comments and constructive suggestions that helps to improve the manuscript. This study is supported by the National Natural Science Foundation of China under grant No. 11390371, 11233004, U1431106, 11573035, 11625313, 11550110492, the National Key Basic Research Program of China (973 program) 2014CB845701. Y.B.K is thankful to the Chinese Academy of Sciences for supporting through CAS PIFI Fellowship. This work has made use of LAMOST data. The Guo Shou Jing Telescope (the Large sky Area Multi-Object fiber Spectroscopic Telescope, LAMOST) is a National Major Scientific Project built by the Chinese Academy of Sciences. Funding for the project has been provided by the National Development and Reform Commission. LAMOST is operated and managed by National Astronomical Observatories, Chinese Academy of Sciences. This research has made use of the VizieR catalogue access tool and the cross-

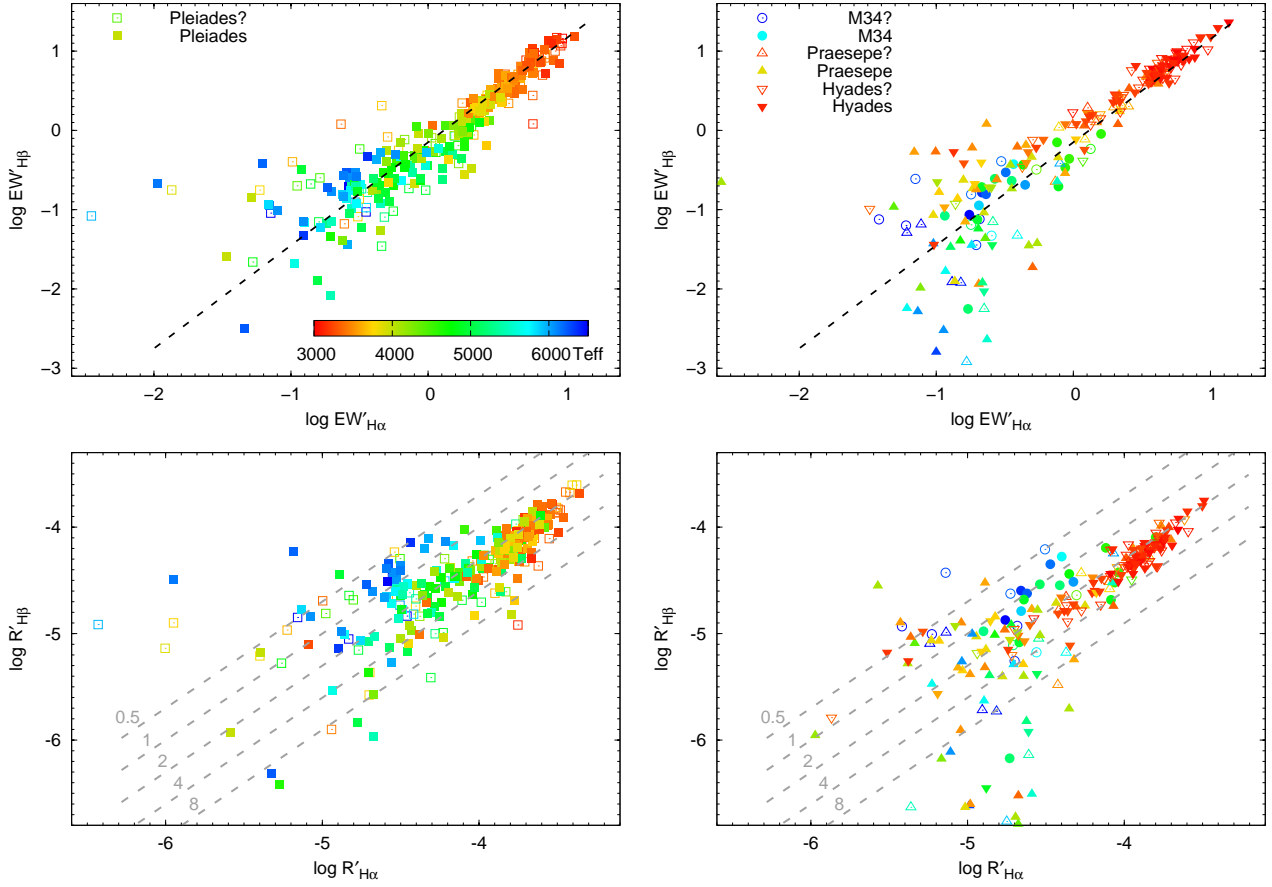


Figure 10. The correlation of excess equivalent widths (upper panels) and fractional excess luminosities (lower panels) of H β and H α lines. Dashed lines in upper panels: power-law approximation (see the text). The dashed lines with grey colours in the lower panels denote constant ratios of $R'_{H\alpha}/R'_{H\beta} = 0.5, 1, 2, 4$ and 8 , respectively.

match service provided by CDS, Strasbourg, France. This research has made use of the WEBDA database, operated at the Department of Theoretical Physics and Astrophysics of the Masaryk University.

REFERENCES

- Agüeros M. A., Covey K. R., Lemonias J. J., et al. 2011, *ApJ*, 740, 110
- An D., Terndrup D. M., Pinsonneault M. H., Paulson D. B., Hanson R. B. & Stauffer J. R. 2007, *ApJ*, 655, 233
- Baliunas S. L., Donahue R. A., Soon W. H., et al., 1995, *ApJ*, 438, 269
- Baliunas S. L., Donahue R. A., Soon W. & Henry G. W. 1998, *Cool Stars, Stellar Systems, and the Sun*, 154, 153
- Barnes S. A. 2003a, *ApJ*, 586, 464
- Barnes S. A. 2003b, *ApJ*, 586, L145
- Bouy H. et al., 2015, *A&A*, 577, 148
- Brandt T. D. & Huang C. X. 2015, *ApJ*, 807, 24
- Canterna R., Crawford D. L., & Perry C. L. 1979, *PASP*, 91, 263
- Carrera R., & Pancino E. 2011, *A&A*, 535, 30
- Charbonneau P. 2014, *ARA&A*, 52, 251
- Chen Y., Girardi L., Bressan A., Marigo P., Barbieri M. & Kong X. 2014, *MNRAS*, 444, 2525
- Copenhagen University, Institute of Astronomy, Cambridge, UK, Real Instituto y Observatorio de la Armada en San Fernando 2011, *yCat*, 1327, 0
- Covey K. R., Agüeros M. A., Law N. M., et al. 2016, *ApJ*, 822, 81
- Cram L. E., & Mullan D. J. 1979, *ApJ*, 234, 579
- Cui X.-Q et al., 2012, *Res. Astron. Astrophys.*, 12, 1197
- Cutri R. M., et al. 2003, *VizieR Online Data Catalog*, 2246, 0
- Delfosse X., Forveille T., Perrier C. & Mayor M. 1998, *A&A*, 1998, 331, 581
- Delorme P., Collier Cameron A., Hebb L., Rostron J., Lister T. A., Norton A. J., Pollacco D. & West R. G. 2011, *MNRAS*, 413, 2218
- Douglas S. T., Agüeros M. A., Covey K. R. 2014, *ApJ*, 795, 161
- Douglas S. T., Agüeros M. A., Covey K. R., Cargile P. A., Barclay T., Cody A., Howell S. B. & Kopytova T. 2016, *ApJ*, 822, 47
- Durney B. R., De Young D. S. & Roxburgh, I. W. 1993, *Solar Physics*, 145, 207
- Fang X.-S., Zhao G., Zhao J.-K., Chen Y.-Q., Bharat Kumar Y., 2016, *MNRAS*, 463, 2494
- Fossati L., Bagnulo S., Landstreet J., Wade G., Kochukhov O., Monier R., Weiss W., Gebran M., 2008, *A&A*, 483, 891
- Gallet F. & Bouvier J. 2013, *A&A*, 556, A36
- Geller A. M., Latham D. W. & Mathieu R. D. 2015, *AJ*, 150, 97
- Gondoin P. 2012, *A&A*, 546, A117
- Gondoin P. 2013, *A&A*, 556, A14
- Gray R. O., Corbally C. J., Garrison R. F., McFadden M. T. & Robinson P. E. 2003, *AJ*, 126, 2048
- Gray R. O., Corbally C. J., Garrison R. F., McFadden M. T., Bubar E. J., McGahee C. E., O'Donoghue A. A. & Knox E. R. 2006, *AJ*, 132, 161

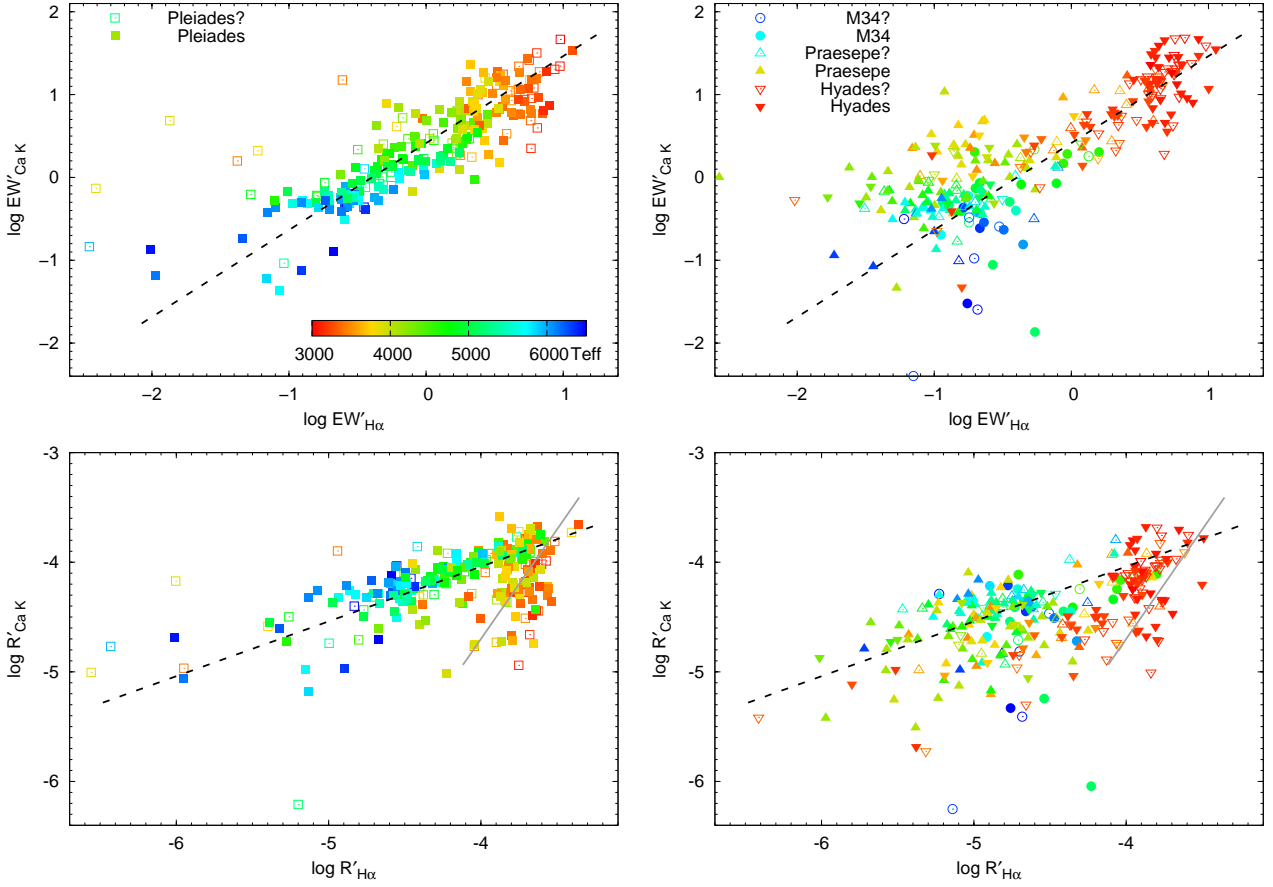


Figure 11. Relationships between excess emissions of H α and Ca II K lines (see the text).

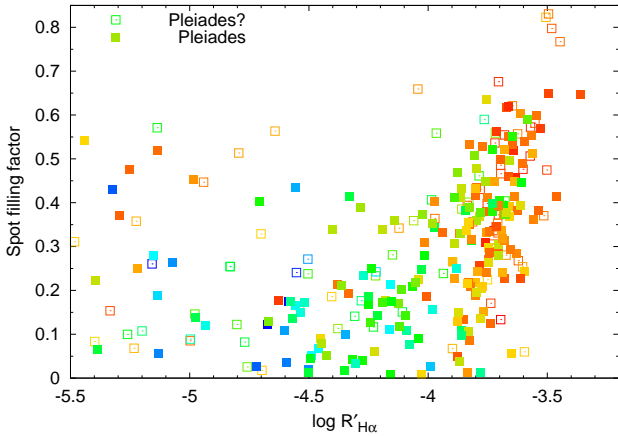


Figure 12. Relations between $R'_{H\alpha}$ and spot filling factor for the Pleiades sample stars with detected cool spots coverage. Colours as in Fig. 9.

Güdel M. 2004, *A&ARv*, 12, 71
 Hall J. C. & Ramsey L. W. 1992, *AJ*, 104, 1942
 Hall J. C. 2008, *Living Rev Solar Phys*, 5, 2
 Hartman J. D., Bakos G. Á., Kovács G., Noyes R. W., 2010, *MNRAS*, 408, 475
 Hartman J. D., Bakos G. Á., Noyes R. W., SipH ocz B., Kovács G., Mazeh T., Shporer A. & Pál A. 2011, *AJ*, 141, 166
 Hawley S. L., Reid I. N., Gizis J. E., & Byrne P. B. 1999, in *Butler*

C. J., Doyle J. G., eds, *ASP Conf. Ser. Vol. 158, Solar and Stellar Activity: Similarities and Differences*. p. 63
 Henry T. J., Soderblom D. R., Donahue R. A. & Baliunas S. L. 1996, *AJ*, 111, 439
 Hodgkin S. T., Jameson R. F., Steele I. A., 1995, *MNRAS*, 274, 869
 Huenemoerder D. P. & Ramsey L. W. 1987, *ApJ*, 319, 392
 Husser T.-O., Wende-von Berg, S., Dreizler S., Homeier D., Reiners A., Barman T. & Hauschildt P. H. 2013, *A&A*, 553, A6
 Irwin J., Aigrain S., Hodgkin S., Irwin M., Bouvier J., Clarke C., Hebb L. & Moraux E. 2006, *MNRAS*, 370, 954
 Jackson R. J. & Jeffries R. D., 2010, *MNRAS*, 407, 465
 Jackson R. J. & Jeffries R. D. 2012, *MNRAS*, 423, 2966
 Jackson R. J. & Jeffries R. D. 2012, *MNRAS*, 431, 1883
 Jacobson H. R., Pilachowski C. A. & Friel E. D. 2011, *AJ*, 142, 59
 James D. J., Barnes S. A., Meibom S., et al. 2010, *A&A*, 515, 100
 Jones B. F. & Prosser C. F. 1996, *AJ*, 111, 1193
 Kovács G., Hartman J. D., Bakos G. Á., et al. 2014, *MNRAS*, 442, 2081
 Lee Y. S., Beers T. C., & Sivarani T., et al. 2008, *AJ*, 136, 2050
 Liu X.-W., Zhao G. & Hou J.-L., 2015, *Res. Astron. Astrophys.*, 15, 1089
 Lockwood G. W., Skiff B. A., & Radick R. R. 1997, *ApJ*, 485, 789
 Lockwood G. W., Skiff B. A., Henry G. W., Henry S., Radick R. R., Baliunas S. L., Donahue R. A. & Soon W. 2007, *ApJS*, 171, 260
 Luo A.-L. et al., 2015, *Res. Astron. Astrophys.*, 15, 1095
 Mamajek E. E. & Hillenbrand L. A. 2008, *ApJ*, 687, 1264

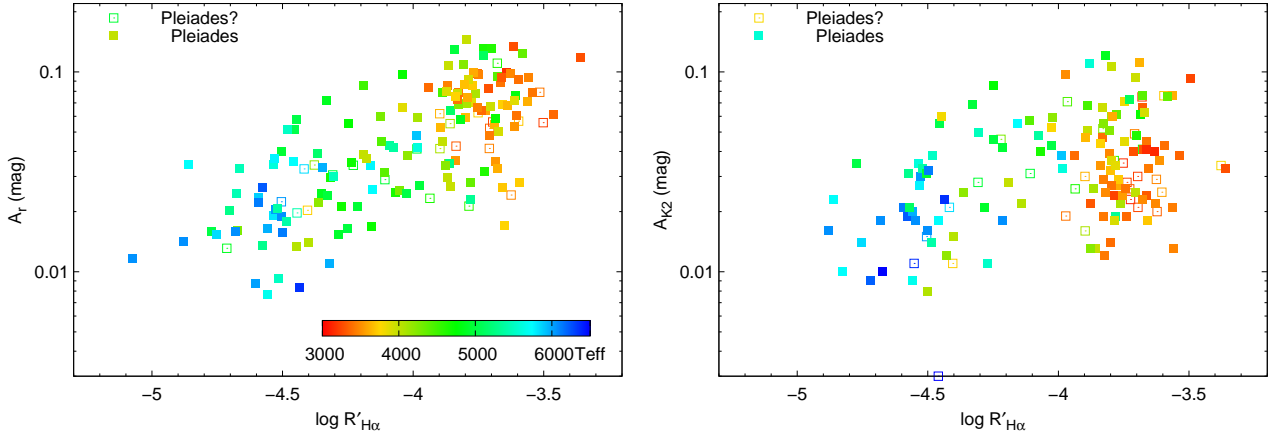


Figure 13. Amplitudes of light variation (left: HATNet, right: K2) as a function of $\log R'_{H\alpha}$. Note that the amplitude is in log scale.

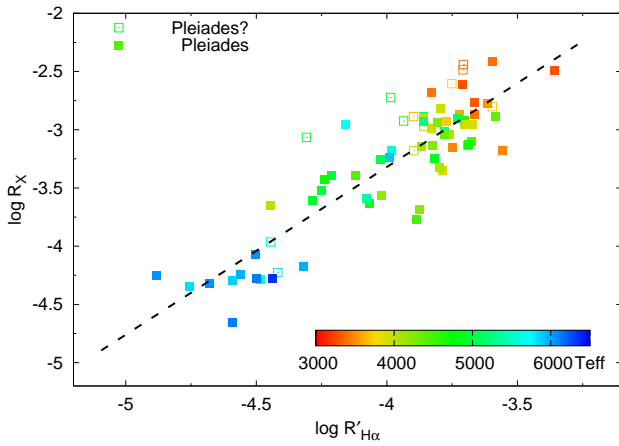


Figure 14. The relations between $H\alpha$ fractional luminosity $R'_{H\alpha}$ and X-ray fractional luminosity R_X .

Marsden S. C., Carter B. D., & Donati J.-F. 2009, MNRAS, 399, 888
 Martínez-Arnáiz, R., López-Santiago, J., Crespo-Chacón, I. & Montes, D. 2011, MNRAS, 414, 2629
 McQuillan A., Mazeh T. & Aigrain S. 2014, ApJS, 211, 24
 Meibom S., Mathieu R. D., Stassun K. G., Liebesny P. & Saar S. H. 2011, ApJ, 733, 115
 Melis C., Reid M. J., Mioduszewski A. J., Stauffer J. R., Bower G. C., 2014, Science, 345, 1029
 Mermilliod J.-C., Mayor M., & Udry S. 2009, A&A, 498, 949
 Montes D., Fernández-Figueroa M. J., de Castro E. & Cornide M. 1995, A&A, 294, 165
 Montes D., Fernández-Figueroa M. J., Cornide M. & de Castro E. 1996, A&A, 312, 221
 Montes D., Crespo-Chacón I., Gálvez M. C., Fernández-Figueroa M. J., López-Santiago J., de Castro E., Cornide M. & Hernán-Obispo M. 2004, Lecture Notes and Essays in Astrophysics, 1, 119
 Newton E. R., Irwin J., Charbonneau D., Berlind P., Calkins M. L. & Mink J. 2017, ApJ, 834, 85
 Noyes R. W., Hartmann L. W., Baliunas S. L., Duncan D. K., Vaughan A. H. 1984, ApJ, 279, 763
 Önehag A., Korn A., Gustafsson B., Stempels E., & Vandenberg D. A. 2011, A&A, 528, A85
 Perryman, M. A. C., Brown, A. G. A., Lebreton, Y., et al. 1998, A&A, 331, 81

Pizzolato N., Maggio A., Micela G., Sciortino S. & Ventura P. 2003, A&A, 397,
 Radick R. R., Thompson D. T., Lockwood G. W., Duncan D. K. & Baggett W. E. 1987, ApJ, 321, 459
 Radick R. R., Lockwood G. W., Skiff B. A. & Baliunas S. L. 1998, ApJS, 118, 239
 Rebull L. M., Stauffer J. R., Bouvier J., et al. 2016, AJ, 152, 113
 Reid N., Hawley S. L. & Mateo M. 1995, MNRAS, 272, 828
 Reiners A., Joshi N. & Goldman B. 2012, AJ, 143, 93
 Reiners A., Schüssler M. & Passegger V. M. 2014, ApJ, 794, 144
 Randich S., Schmitt J. H. M. M., Prosser C. F. & Stauffer J. R. 1996, A&A, 305, 785
 Salaris M., Weiss A., & Percival S. M. 2004, A&A, 414, 163
 Scholz A. & Eislöffel J. 2007, MNRAS, 381, 1638
 Scholz A., Irwin J., Bouvier J., SipH och B. M., Hodgkin S. & Eislöffel J. 2011, MNRAS, 413, 2595
 Schrijver C. J., Dobson A. K., & Radick R. R. 1992, A&A, 258, 432
 Schuler S. C., King J. R., Fischer D. A., Soderblom D. R., & Jones B. F. 2003, AJ, 125, 2085
 Smolinski J. P., Lee Y. S., Beers T. C., et al. 2011, AJ, 141, 89
 Soderblom D. R., Stauffer J. R., Hudon J. D., Jones B. F., 1993, ApJS, 85, 315
 Soderblom, D. R., Jones, B. F. & Fischer, D. 2001, ApJ, 563, 334
 Soderblom D. R., Laskar T., Valenti J. A., Stauffer J. R., Rebull L. M., 2009, AJ, 138, 1292
 Spiegel E. A. & Zahn J.-P. 1992, A&A, 265, 106
 Stauffer J. R. & Hartmann L. W. 1986, ApJS, 61, 531
 Stauffer J. R. & Hartmann L. W. 1987, ApJ, 318, 337
 Stauffer J. R., Giampapa M. S., Herbst W., Vincent J. M., Hartmann L. W. & Stern R. A. 1991, ApJ, 374, 142
 Stauffer J. R., Balachandran S. C., Krishnamurthi A., Pinsonneault M., Terndrup D. M. & Stern R. A. 1997, ApJ, 475, 604
 Stauffer J. R., Schultz G. & Kirkpatrick J. D. 1998, ApJ, 499, L199
 Stauffer J. R., Hartmann L. W., Fazio, G. G., et al. 2007, ApJS, 172, 663
 Taylor B. J., & Jone M. D. 2005, ApJS, 159, 100
 Taylor B. J. 2006, AJ, 132, 2453
 van Leeuwen, F. 2009, A&A, 497, 209
 Vaughan A. H. & Preston G. W. 1980, PASP, 92, 385
 Walkowicz L. M., Hawley S. L., & West A. A. 2004, PASP, 116, 1105
 West A. A., Hawley S. L., Walkowicz L. M., et al. 2004, AJ, 128, 426
 West A. A., & Hawley S. L. 2008, PASP, 120, 1161

Table A1. Equivalent width measurements of H α , H β and Ca II K lines

Line	Line bandpass (Å)	Pseudo-continua (Å)
H α	6557-6569	6547-6557, 6570-6580
H β	4855-4867	4842-4852, 4873-4883
Ca II K	3930-3937	3910-3915, 3950-3955

- West A. A., Hawley S. L., Bochanski J. J., Covey K. R., Reid I. N., Dhital S., Hilton E. J. & Masuda M. 2008, *AJ*, 135, 785
- West A. A., Weisenburger K. L., Irwin J., Berta-Thompson Z. K., Charbonneau D., Dittmann J. & Pineda J. S. 2015, *ApJ*, 812, 3
- Wilson O. C. 1968, *ApJ*, 153, 221
- Wilson O. C. 1978, *ApJ*, 226, 379
- Wright N. J., Drake J. J., Mamajek E. E. & Henry G. W. 2011, *ApJ*, 743, 48
- Wright N. J. & Drake J. J. 2016, *Nature*, 535, 526
- Wu Y., Luo A.-L., Li H.-N., et al. 2011, *Res. Astron. Astrophys.*, 11, 924
- Yang X. L., Chen Y. Q. & Zhao G. 2015, *AJ*, 150, 158
- Zacharias N., et al. 2012, *VizieR Online Data Catalog*, 1322, 0
- Zhao G., Chen Y.-Q., Shi J.-R., Liang Y.-C., Hou J.-L., Chen L., Zhang H.-W. & Li A.-G., 2006, *ChJAA*, 6, 265
- Zhao G., Zhao Y.-H., Chu Y.-C., Jing Y.-P., Deng L.-C., 2012, *Res. Astron. Astrophys.*, 12, 723

APPENDIX A: CHROMOSPHERIC INDICATORS: Ca II K, H β

We measured equivalent widths of Ca II K and H β lines, $EW_{Ca\ K}$ and $EW_{H\beta}$, and wavelength regime for these measurements are listed in Table A1. To get reliable measurements for these two blue lines, we merely measured $EW_{Ca\ K}$ for stars with g -band signal-to-noise ratio $SNR_g > 1.0$, and measured $EW_{H\beta}$ for those with $SNR_g > 3.0$. Such SNR_g trim criteria cut off about 18 percent and 3 percent of total sample stars, for Ca II K and H β , respectively. Fig. A1 shows the measurements of $EW_{Ca\ K}$ and $EW_{H\beta}$ as a function of effective temperature. Note that the corresponding basal values are also plotted, which were derived based on a large sample of inactive reference dwarf stars with solar metallicity, following the similar procedure that used to derive mean basal values for H α (see Paper I for more details). Similar to $EW'_{H\alpha}$, we obtained the excess equivalent widths of the Ca II K and H β lines, $EW'_{Ca\ K}$ and $EW'_{H\beta}$, respectively. Further, we derived the excess fractional luminosities, $R'_{Ca\ K} (\equiv L'_{Ca\ K}/L_{bol})$ and $R'_{H\beta} (\equiv L'_{H\beta}/L_{bol})$, by using corresponding χ ratios (see Appendix C). These measurements are shown in bottom panels of Fig. A1.

Note that the derived mean value of inactive reference stars cut off at 6500 K. However, a very small fraction of sample stars are hotter than 6500 K (see Fig. 1). We simply linearly extrapolated the reference value when necessary. In order to get reliable measurements for sample stars with $T_{eff} > 6500$ K, we merely derived the excess equivalent widths for those stars with T_{eff} less than 6900 K in this work.

APPENDIX B: MEASUREMENT UNCERTAINTIES

The uncertainties in the equivalent width measurements mainly result from the errors in the RV-corrected LAMOST spectra. The uncertainty in the LAMOST spectra at each wavelength (Poisson noise, and any noises during data reduction) is available and was directly propagated to the equivalent width measurements. Fig. B1 shows the errors ($\sigma_{EW_{H\alpha}}$) in $EW_{H\alpha}$ for stars in each open cluster, and the increment in errors with decreasing temperature is seen as expected. The typical error of $EW_{H\alpha}$ is less than 0.1 Å for GK-type sample stars, e.g., ~ 0.05 Å for Pleiades members with temperatures around 5000 K; however, it become large for M-type stars, e.g., typically greater than 0.1 Å and up to 0.5 Å. Also, the lower SNR in the blue band of spectra increases the uncertainties in the measurements of Ca II K and H β lines, especially for those M-type stars, e.g., the typical errors of $EW_{H\beta}$ are 0.05, 0.15, 1.0 Å, for Pleiades members with temperatures around 5500, 4500, 3500 K, respectively.

The spectral resolution of LAMOST spectra ($R \sim 1800$) limits the accuracy of RV measurements. To check how RV uncertainties affect $EW_{H\alpha}$ measurements, we have taken PHOENIX model spectra and degraded the resolution to 1800 by convolving a Gaussian profile, found that the differences of $EW_{H\alpha}$ due to RV shifts of ± 20 $km\ s^{-1}$ are less than 0.02 Å (a relative difference of less than 3 percent), as shown in Fig. B2. In addition, many cool Pleiades members are fast rotators (Rebull et al. 2016), we thus evaluated the effects of rotational broadening on measurements of $EW_{H\alpha}$, and found the differences of $EW_{H\alpha}$ due to a $v \sin i$ of ~ 100 $km\ s^{-1}$ are typically less than 0.04 Å (see Fig. B2), which is slightly larger than the errors due to RV uncertainties, but typically less than average errors of $EW_{H\alpha}$ measurements propagated from the uncertainties of the observed flux. So the uncertainties from RV-correction and rotational broadening are marginal compared to those due to uncertainty of observed spectra.

The uncertainties in $EW'_{H\alpha}$ are mainly propagates from the errors of $EW_{H\alpha}$ measurement and corresponding basal value used at a given temperature. The basal value of equivalent width for a given line was derived based on a large sample of reference dwarfs with solar metallicity (e.g., for H α line, see Paper I). The scatter of $EW_{H\alpha}$ of reference stars in each 50 K bin is typically smaller than the errors of measured $EW_{H\alpha}$, as demonstrated in the upper panels of Fig. 2, where three times of the scatter ($\pm 3\sigma$) are shown in grey lines. To estimate the uncertainties on the derived $EW'_{H\alpha}$ resulting from the flux errors of spectra and uncertainties of temperature, we performed a Monte Carlo simulation 1000 times for six representative $EW_{H\alpha}$ values with T_{eff} from 6000 to 3500 K, using the typical measurement error (see Fig. B1) as the standard deviation of $EW_{H\alpha}$, and setting 100 K as the standard deviation of temperature, as shown in Fig. B3 and listed in Table B1. It is clear that the $EW'_{H\alpha}$ uncertainties are dominated by the uncertainties of temperatures for GK-type stars. It is not the same case with M-type stars since the reference $EW_{H\alpha}$ value is not so sensitive to temperature compared to hotter stars.

The excess fractional luminosity $R'_{H\alpha}$ depends on both derived $EW'_{H\alpha}$ and estimated value of χ at a given temperature. To check the temperature selection affect on derived

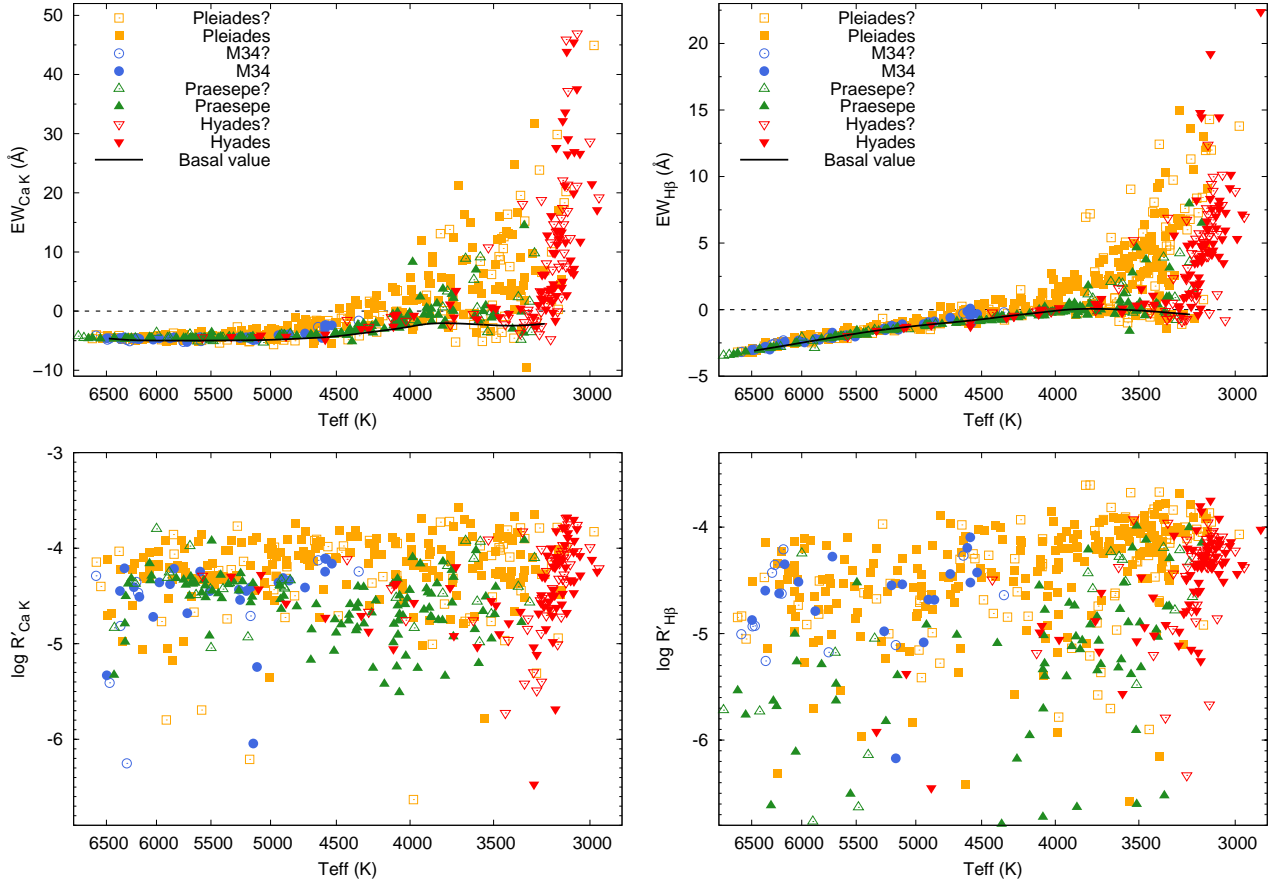


Figure A1. Emissions of $H\beta$ and $Ca\ II\ K$ lines for all sample stars.

Table B1. Estimated uncertainties from Monte Carlo simulations

Teff (σ) (K)	EW $_{H\alpha}$ (σ) (Å)	σ_1 (Å)	σ_2 (Å)	σ_3 (dex)	σ_4 (dex)	σ_5 (dex)
6000(100)	-2.0(0.03)	0.09	0.10	0.08	0.19	0.20
5500(100)	-1.0(0.04)	0.12	0.12	0.03	0.08	0.08
5000(100)	0.0(0.05)	0.09	0.10	0.02	0.04	0.04
4000(100)	2.0(0.10)	0.09	0.13	0.02	0.04	0.05
3500(100)	4.0(0.20)	0.06	0.22	0.02	0.06	0.07
4500(100)	0.0(0.07)	0.08	0.11	0.04	0.06	0.08
4500(100)	1.0(0.07)	0.08	0.11	0.02	0.03	0.04
4500(100)	2.0(0.07)	0.08	0.11	0.01	0.03	0.03

σ_1 : $\sigma(EW'_{H\alpha})$ due to $\sigma(T_{\text{eff}})$;

σ_2 : $\sigma(EW'_{H\alpha})$ due to both $\sigma(EW_{H\alpha})$ and $\sigma(T_{\text{eff}})$;

σ_3 : $\sigma(\log R'_{H\alpha})$ due to $\sigma(EW_{H\alpha})$;

σ_4 : $\sigma(\log R'_{H\alpha})$ due to $\sigma(T_{\text{eff}})$;

σ_5 : $\sigma(\log R'_{H\alpha})$ due to both $\sigma(EW_{H\alpha})$ and $\sigma(T_{\text{eff}})$.

$R'_{H\alpha}$, we performed a simple Monte Carlo simulations (see Table B1), which show that temperature uncertainty dominates the derived $R'_{H\alpha}$ uncertainty, as shown in Fig. B3.

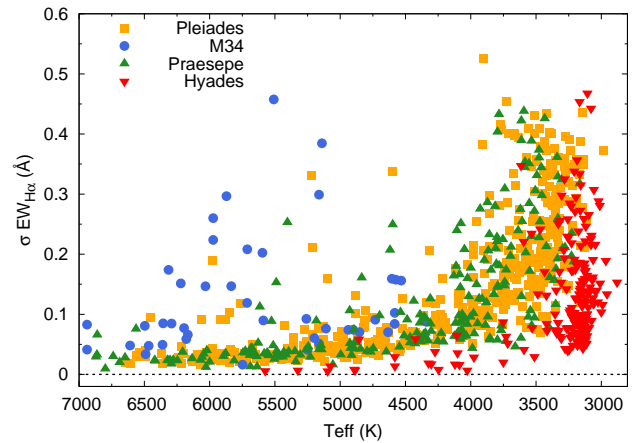


Figure B1. Errors in measurements of $EW_{H\alpha}$. Note Hyades members have smaller errors because of the proximity.

APPENDIX C: THE RATIO OF THE CONTINUUM FLUX TO THE BOLOMETRIC FLUX

To quantify the strength of chromospheric activity as the ratio between $H\alpha$ emission luminosity and bolometric luminosity, Walkowicz, Hawley & West (2004) introduced a distance-independent value χ , the ratio between the appar-

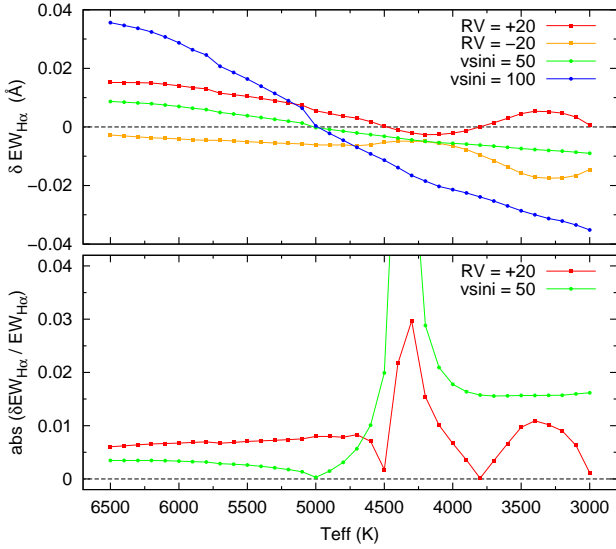


Figure B2. Top: Estimated differential $EW_{H\alpha}$ values due to wavelength shifts, $RV = \pm 20 \text{ km s}^{-1}$, and rotational broadening, $v \sin i = 50$ and 100 km s^{-1} . Bottom: Relative differences compared to $EW_{H\alpha}$ scales, note that the large values around 4300 K result from the fact that $EW_{H\alpha}$ is near to zero for late K-type stars.

ent continuum flux near $H\alpha$, $f(\lambda_{6560})$, and the apparent bolometric flux, f_{bol} , namely, $\chi = f(\lambda_{6560})/f_{\text{bol}}$. Then the measured equivalent width of $H\alpha$ emission line could be converted to the fractional luminosity by using the χ value, i.e., $L_{H\alpha}/L_{\text{bol}} = \chi \times EW_{H\alpha}$. χ -method is widely used where flux-calibrated spectrum and distance information is not available for quantifying chromospheric activity level (e.g., Douglas et al. 2014; West et al. 2015).

χ values could be estimated based on observed spectra (e.g. West & Hawley 2008) or model spectra (e.g. Reiners, Joshi & Goldman 2012). In this work, we estimated the χ values as the ratio of the surface continuum flux, $F(\lambda_c)$, to the stellar surface bolometric flux, F_{bol} , using the following formula,

$$\chi = \frac{F(\lambda_c)}{F_{\text{bol}}} = \frac{F(\lambda_c)}{\sigma T_{\text{eff}}^4}, \quad (\text{C1})$$

where σ is Stefan-Boltzmann constant, $\sigma \approx 5.6704 \times 10^{-5} \text{ erg s}^{-1} \text{ cm}^{-2} \text{ K}^{-4}$. We evaluated $F(\lambda_c)$ for the lines of interest using PHOENIX ACES model spectra with solar metallicity (Husser et al. 2013). We then obtained χ values for $H\alpha$, Ca II K and $H\beta$ lines, as shown in Fig. C1.

To check the agreement of these χ values derived from models with those from the observations, we collected the flux calibrated SDSS spectra of stars in NGC 2420, M 67, and Praesepe. 140 members of NGC 2420 with $\log g > 4.0$ and 52 dwarfs in M 67 were selected from the catalogue of Lee et al. (2008). We estimated their radii using the temperatures from Lee et al. (2008), adopting the PARSEC model (Chen et al. 2014) with a metallicity of $[\text{Fe}/\text{H}] \sim -0.2$ (Jacobson, Pilachowski & Friel 2011) and an age of ~ 2 Gyr (Salaris, Weiss & Percival 2004), and the PARSEC model with a solar metallicity (Jacobson, Pilachowski & Friel 2011) and an age of ~ 4 Gyr (Önehag et al. 2011; Geller, Latham & Mathieu 2015), for NGC 2420 and M67 respectively. We collected SDSS

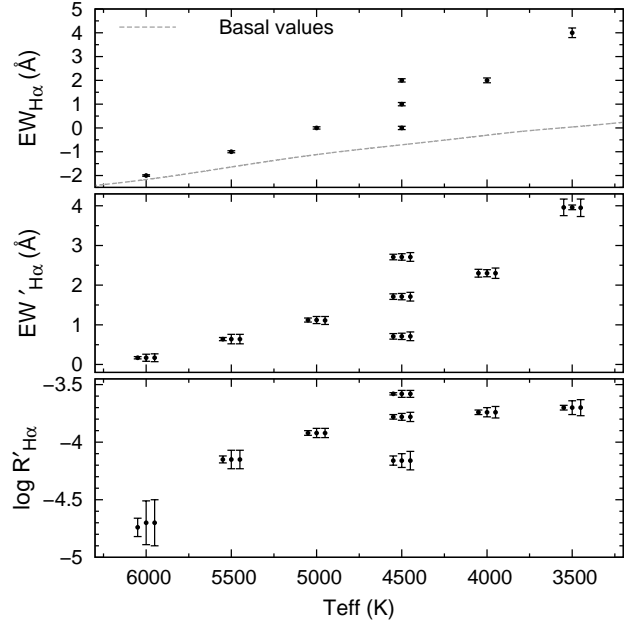


Figure B3. Top: Examples of typical values of $EW_{H\alpha}$ with measured errorbars $\sigma(EW_{H\alpha})$. Middle and bottom: Resulted excess emissions with estimated errorbars from different uncertainty sources by using Monte Carlo simulations. The data points at the same temperature are separated by 50 K for display purpose: uncertainties from $EW_{H\alpha}$ (left), from T_{eff} (centre), and from both of them (right).

spectra with good quality ($SNR > 10$) for 36 Praesepe stars of Douglas et al. (2014) based on the SDSS DR12 SSPP output catalogue (Lee et al. 2008; Smolinski et al. 2011). We estimated their effective temperatures using the colours ($V - K_s$ and/or $r - K_s$), and derived corresponding radii adopting the PARSEC model with a metallicity of $[\text{Fe}/\text{H}] \sim +0.16$ (Carrera & Pancino 2011) and an age of about 650 Myr. The distances adopted from WEBDA (<http://www.univie.ac.at/webda/>) for NGC 2420, M 67 and Praesepe are 3085, 908 and 187 pc, respectively. Based on the observed continuum flux, $f(\lambda_c)$, and their corresponding radii (R) and distances (D), the χ ratios could be derived using the following relation,

$$\chi = \frac{F(\lambda_c)}{F_{\text{bol}}} = \frac{(D/R)^2 f(\lambda_c)}{\sigma T_{\text{eff}}^4}, \quad (\text{C2})$$

as shown in Fig. C1, wherein the error bar is equivalent to its uncertainty due to 10 percent error of distance. There exists a slight offset between members in NGC 2420 and M 67 at the same effective temperatures, which may be due to the uncertainties in distance, and/or the difference in basic physical parameters between these two clusters. Also shown in Fig. C1 by the red dashed line is a relation for $H\alpha$ line, which was derived from empirically determined surface flux of $H\alpha$ line provided by Soderblom et al. (1993). As shown by the figure, the χ values from model spectra are overall in good agreement with those from observations, there however exist some small discrepancies between them, e.g., ~ 0.1 dex in $H\alpha$ line around 4500 K.

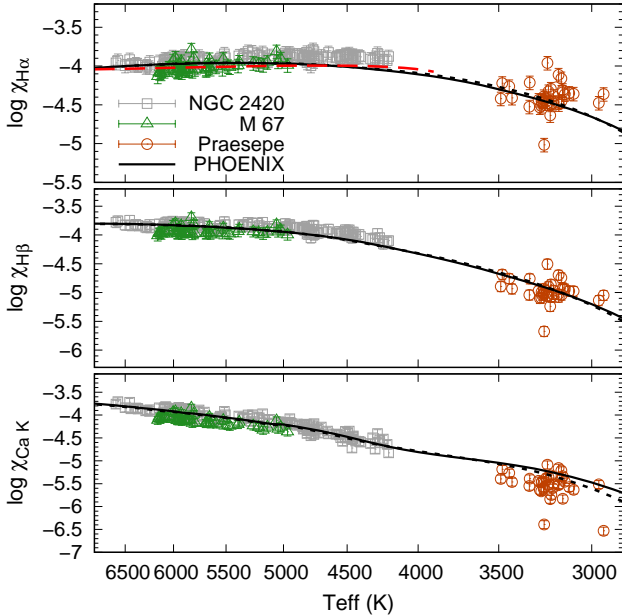


Figure C1. χ values of $H\alpha$, $H\beta$, and Ca II K lines, $\chi_{H\alpha}$, $\chi_{H\beta}$, and $\chi_{\text{Ca K}}$, respectively, derived based on SDSS spectra, and PHOENIX model spectra with $\log g=4.5$ (black solid lines) and $\log g=5.0$ (black dashed lines). The red long dashed line denotes the relation derived from empirically determined $H\alpha$ line surface flux provided by [Soderblom et al. \(1993\)](#).

APPENDIX D: ESTIMATE OF QUIESCENT PHOTOSPHERE TEMPERATURE AND MASS

The cool spots on the stellar surface contribute light that would affect spectral features and broad-band colours, for which the derived effective temperature becomes the average surface temperature (flux-weighted mean temperature) in spotted stars. Therefore, no direct way to derive a quiescent temperature for active stars, particularly those Pleiades members with large spot coverages (see Paper I for more discussion on this topic).

For Pleiades members, we followed the procedures in Paper I to estimate the quiescent temperature (see Paper I for more details). For M34 members, we collected V band magnitudes from literature ([Jones & Prosser 1996](#); [Irwin et al. 2006](#); [Meibom et al. 2011](#)), and got their K_s -band magnitudes from 2MASS archive ([Cutri et al. 2003](#)) via Vizier x-match service. We estimated their quiescent temperatures based on $V - K_s$ colours using PARSEC isochrones ([Chen et al. 2014](#)) with an age of 220 Myr and solar metallicity, wherein we adopted the reddening of $E(B-V)=0.07$ mag ([Canterna, Crawford & Perry 1979](#)).

For Praesepe and Hyades candidates, firstly we derived their effective temperatures based on $V - K_s$ colours, where V magnitudes taken from the fourth U.S. Naval Observatory CCD Astrograph Catalogue (UCAC4; [Zacharias et al. 2012](#)). A small fraction of sample stars have no V magnitudes, we then derived their temperatures based on $r - K_s$, where r magnitudes from the Carlsberg Meridian Catalogue 15 (CMC15; [Copenhagen University et al. 2011](#)). The PARSEC models with an age of 650 Myr and a metallicity of $[\text{Fe}/\text{H}]\sim 0.1$ were used to convert colours to temper-

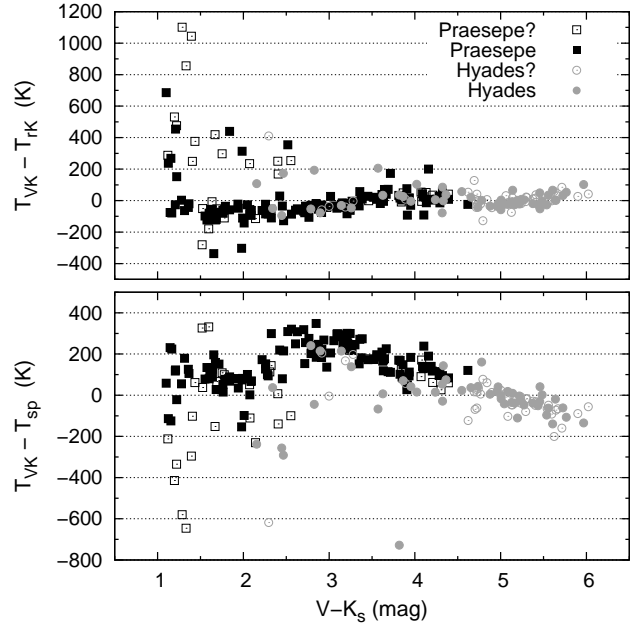


Figure D1. The differences between $V - K_s$ -based temperature (T_{VK}), $r - K_s$ -based temperature (T_{rK}), and the temperature from spectral features (T_{sp}) among stars in Praesepe and Hyades.

atures, where the reddening $E(B-V) = 0^m.027$ and $E(B-V)=0^m.001$ ([Taylor 2006](#)) were adopted for Praesepe and Hyades, respectively. We then compared the colour-based temperatures with the spectra-based temperatures (T_{sp} , for FGK-type stars, we adopt the values provided by LASP, for M-type stars, we derived it via the molecular band CaH using the method in Paper I), and found that there exist complex differences between colour-based temperatures and spectra-based temperatures, as shown in Fig. D1. We finally adopted the effective temperatures from spectral features as the quiescent temperatures for stars in these two clusters.

For the M-type slow rotators in Kepler field, firstly we estimated temperature for each target based on the molecular bands of CaH and TiO following the method in Paper I, and then took the average of our measured value and the value provided by [McQuillan, Mazeh & Aigrain \(2014\)](#), as finally adopted quiescent temperature.

To identify potential binaries and non-members for the member candidates in open clusters, we followed the procedures used in Paper I by using available CMDs, e.g., we identified these stars as photometrically binaries/non-members that have larger deviation compared with empirical single-star loci in V vs. $V - K_s$ diagram, namely, brighter stars with $-1^m.0 < \Delta V < -0^m.5$ were classified as probable binary members, while the fainter stars with $\Delta V > 0^m.3$ or very much brighter stars with $\Delta V < -1^m.0$ were identified as probable non-member stars.

Once the effective temperatures are obtained for each star, we estimated the mass from temperature based on mass- T_{eff} relation from PARSEC isochrones ([Chen et al. 2014](#)). Note that, for these M-stars in Kepler field, we used the isochrones with a solar metallicity and an age of 2 Gyr.

APPENDIX E: ROTATION PERIODS COLLECTION

For Pleiades, [Hartman et al. \(2010\)](#) detected rotation periods for nearly 400 members using the Hungarian-made Automated Telescope Network (HATNet) transit survey data. Recent studies based on dedicated photometric surveys, e.g., the Palomar Transient Factory (PTF) ([Covey et al. 2016](#)), and the *K2* ([Rebull et al. 2016](#)), increased the measurements of rotation periods for more than 500 new members of this open cluster, vastly expanding the number of Pleiades members with rotation periods. For these members with multi-rotation measurements, we adopted values from the *K2* ([Rebull et al. 2016](#)), and for others, we adopted their rotation periods provided by [Covey et al. \(2016\)](#) and [Hartman et al. \(2010\)](#). Totally, 231 Pleiades members in our sample have available rotation periods.

For M34, we collected rotation periods from literature, [Irwin et al. \(2006\)](#); [James et al. \(2010\)](#); [Meibom et al. \(2011\)](#). The latest measurements were adopted in this paper. Totally, we found 21 members have rotation periods.

For stars in Praesepe, their rotation periods were collected from [Scholz & Eislöffel \(2007\)](#); [Delorme et al. \(2011\)](#); [Scholz et al. \(2011\)](#); [Agüeros et al. \(2011\)](#); [Kovács et al. \(2014\)](#). Totally, we got their rotation periods for 76 stars in Praesepe sample. For Hyades, we collected the rotation periods from [Radick et al. \(1987\)](#); [Delorme et al. \(2011\)](#); [Hartman et al. \(2011\)](#); [Douglas et al. \(2016\)](#). Totally, 24 stars in Hyades sample have rotation periods.

APPENDIX F: ON-LINE TABLES

We compiled the measurements for stars in Pleiades, M34, Praesepe and Hyades in on-line Table F1-F4, respectively, including effective (quiescent) temperatures, equivalent widths of $H\alpha$, $H\beta$ and Ca II K lines, their excess equivalent widths, excess fractional luminosities, and spot filling factors.

This paper has been typeset from a $\text{\TeX}/\text{\LaTeX}$ file prepared by the author.